Miner Deposita (2006) 41: 607–636
DOI 10.1007/s00126-006-0061-y

ARTICLE

M. Simard · G. Beaudoin · J. Bernard · A. Hupé

Metallogeny of the Mont-de-l'Aigle IOCG deposit, Gaspé Peninsula, Québec, Canada

Received: 10 October 2005 / Accepted: 25 March 2006 / Published online: 22 August 2006

Abstract The Mont-de-l'Aigle deposit is located in the northern part of Dome Lemieux, in the Connecticut Valley-Gaspé Synclinorium, Gaspé Peninsula, Québec. The Dome Lemieux is a subcircular antiform of Siluro–Devonian sedimentary rocks that is cut by numerous mafic and felsic sills and dikes of Silurian to Late Devonian age. Plutonism occurred in a continental within-plate extensional setting typical of orogenic collapse. The Cu−Fe (± Au) mineralization of Mont-de-l'Aigle occurs in veins, stockworks, and breccias. Mineralization is located near or within N−S and NW−SE faults cutting sedimentary rocks. IOCG mineralization postdates intrusions, skarns, hornfels, and epithermal mineralization typical of the southern part of the Dome Lemieux. The paragenetic sequence comprises: (1) pervasive sodic, potassic, chlorite, and silica alteration, (2) hematite, quartz, pyrite, magnetite, and chalcopyrite veins, stockworks and breccias and, (3) dolomite ± hematite veins and veinlets cutting the earlier mineralization. Intrusions display proximal sodic and potassic alteration, whereas sedimentary rocks have proximal decalcification, silicification, and potassic alteration. Both intrusive and sedimentary rocks are affected by a pervasive distal chlorite (± silica) alteration. The sulfur isotope composition of pyrite and chalcopyrite ($\delta^{34}S$=−1.5 to 4.8‰) suggests that sulfur was derived mainly from igneous rocks. Fluid $\delta^{18}O$ (−0.4 to 2.65‰) indicates meteoric or seawater that reacted with the country rocks. Mixing of hot magmatic fluids with a cooler fluid, perhaps meteoric or seawater is suggested for mineral deposition and alteration of the Mont-de-l'Aigle deposit. The mineralogy, alteration, and sulfur isotope composition of the Mont-de-l'Aigle deposit compare well with IOCG deposits worldwide, making the Mont-de-l'Aigle deposit a rare example of Paleozoic IOCG mineralization, formed at shallow depth, within a low metamorphic grade sedimentary rock sequence.

Keywords Gaspé Peninsula · Dome Lemieux · IOCG deposits · Hematite · Breccia

Editorial handling: D. Lentz

M. Simard · G. Beaudoin (✉) · J. Bernard
Département de Géologie et de Génie Géologique,
Université Laval,
Sainte-Foy, QC, G1K 7P4, Canada
e-mail: georges.beaudoin@ggl.ulaval.ca
Tel.: +1-418-6563141
Fax: +1-418-6567339

A. Hupé
Ressources Appalaches,
212 Avenue de la Cathédrale,
Rimouski, QC, G5L 5J2, Canada

Introduction

The Cu–Fe (± Au) Mont-de-l'Aigle deposit is characterized by copper–iron oxide veins, stockworks and breccias hosted by Siluro–Devonian sedimentary and volcanic rocks cut by Silurian to Late Devonian mafic and felsic intrusions. The Mont-de-l'Aigle showings are copper- and iron-rich with gold values up to 2.2 g/t. Mineralization is associated spatially with faults and mafic to felsic intrusions, and consists of abundant hematite and large breccia bodies with hematite–quartz cement. Many of the features of the Mont-de-l'Aigle deposit are consistent with iron oxide–copper–gold deposits (IOCG) (Hitzman et al. 1992; Hitzman 2000; Williams et al. 2005). However, the Paleozoic age of carbonate-host rocks of the Mont-de-l'Aigle deposit is atypical for IOCG deposits (Hitzman et al. 1992). IOCG deposits constitute new exploration targets in the Appalachian belt.

IOCG deposits have become attractive exploration targets and the subject of intense research. IOCG deposits were first defined by Hitzman et al. (1992) as the shallow crustal expression of deep-seated, volatile-rich igneous-hydrothermal systems. Scientific debate on the origin of IOCG deposits includes both metal-bearing magmatic brines (Hitzman et al. 1992; Pollard 2002) and external basinal brines heated by intrusions (Barton and Johnson 1996; Hitzman 2000) being proposed as hydrothermal fluid end-members. Barton and Johnson (1996) proposed that some igneous-related IOCG deposits formed by hydro-

thermal brines derived either from coeval salars or older evaporites. Hitzman (2000) concluded that the critical factor for making an IOCG deposit is the influx of nonmagmatic, oxidized, saline, and copper-rich fluids. IOCG deposits range in age from Archean for the Salobo and Igarapé Bahia districts in Brazil (Requia et al. 2003; Tallarico et al. 2005), to Jurassic–Cretaceous for the Chilean Iron Belt and El Laco districts in Chile (Marschick and Fontboté 2001), but they are dominantly Middle Proterozoic in age (Hitzman et al. 1992).

The host rocks range from granite to clastic sedimentary rocks, mafic to felsic volcanic, and volcanosedimentary rocks metamorphosed from greenschist to amphibolite grades (Hitzman et al. 1992). IOCG deposits form in three tectonic environments: (1) intracontinental, continental orogenic collapse; (2) intracontinental anorogenic magmatism; and (3) extension along a subduction-related continental margin (Hitzman 2000). The range of proposed hydrothermal fluids and processes, and the diversity of geological environments where these deposits formed, result in the wide variety of deposit styles and mineralogy (Hitzman 2000). Therefore, better understanding of the genesis of IOCG deposits will provide improved guidelines for mineral exploration.

This paper presents the geochemistry of intrusive rocks, mineralogy, paragenetic sequence, hydrothermal alteration, and stable isotope data of the Mont-de-l'Aigle deposit, Gaspé Peninsula, Québec. These data are used to interpret the relationships between the tectonic setting, fluid processes, oxide and sulfide precipitation, and alteration, to demonstrate that the Mont-de-l'Aigle deposit has characteristics similar to IOCG deposits.

Regional geology

The Gaspé Peninsula is a segment of the Canadian Appalachians that formed as a result of terrane accretion to the North American craton during the Paleozoic (Williams and Hatcher 1983; Bourque et al. 1995). The Siluro–Devonian rocks of the Gaspé Peninsula are divided into three major structural zones;

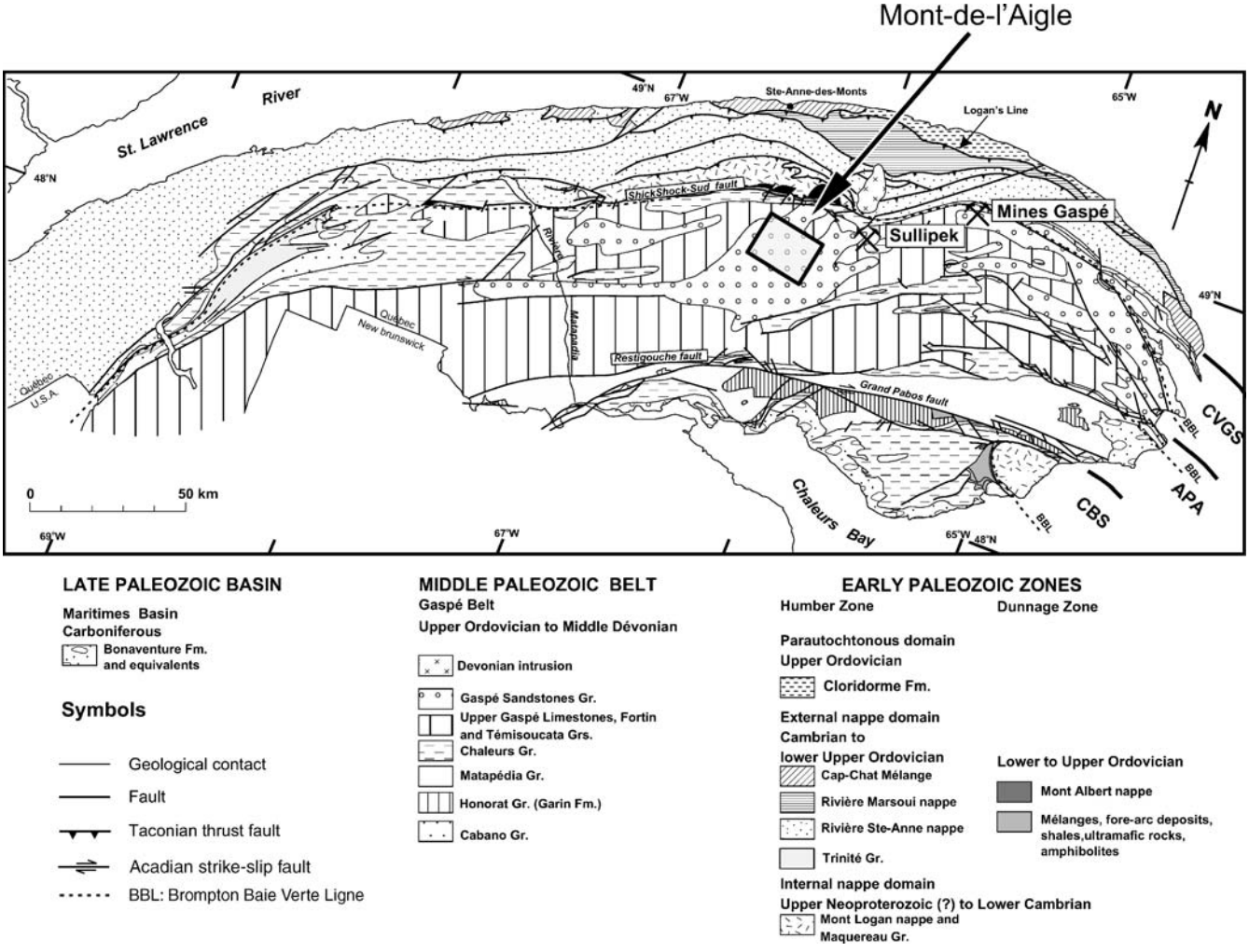

Fig. 1 Geology of the Gaspé Peninsula, Québec Appalachians, with location of the Mont-de-l'Aigle deposit, Sullipek, and Mines Gaspé porphyry copper and skarn deposits (modified from Malo 2001). *CVGS* Connecticut Valley–Gaspé Synclinorium, *APA* Aroostook–Percé Anticlinorium, *CBS* Chaleurs Bay Synclinorium

that, from north to south are (1) the Connecticut Valley-Gaspé Synclinorium, (2) the Aroostook-Percé Anticlinorium, and (3) the Chaleurs Bay Synclinorium (Fig. 1; Malo and Bourque 1993). The Connecticut Valley-Gaspé Synclinorium lies between the Cambro-Ordovician allochtonous rocks of the Taconian Orogen to the northwest and the Aroostook-Percé Anticlinorium to the southeast. It is bounded to the north by the Shickshock-Sud fault, a dextral strike-slip fault (Malo and Bourque 1993), and by the Restigouche fault to the south (Fig. 1). The stratigraphic succession in the Connecticut Valley-Gaspé Synclinorium consists of shallow marine clastic, carbonate and minor

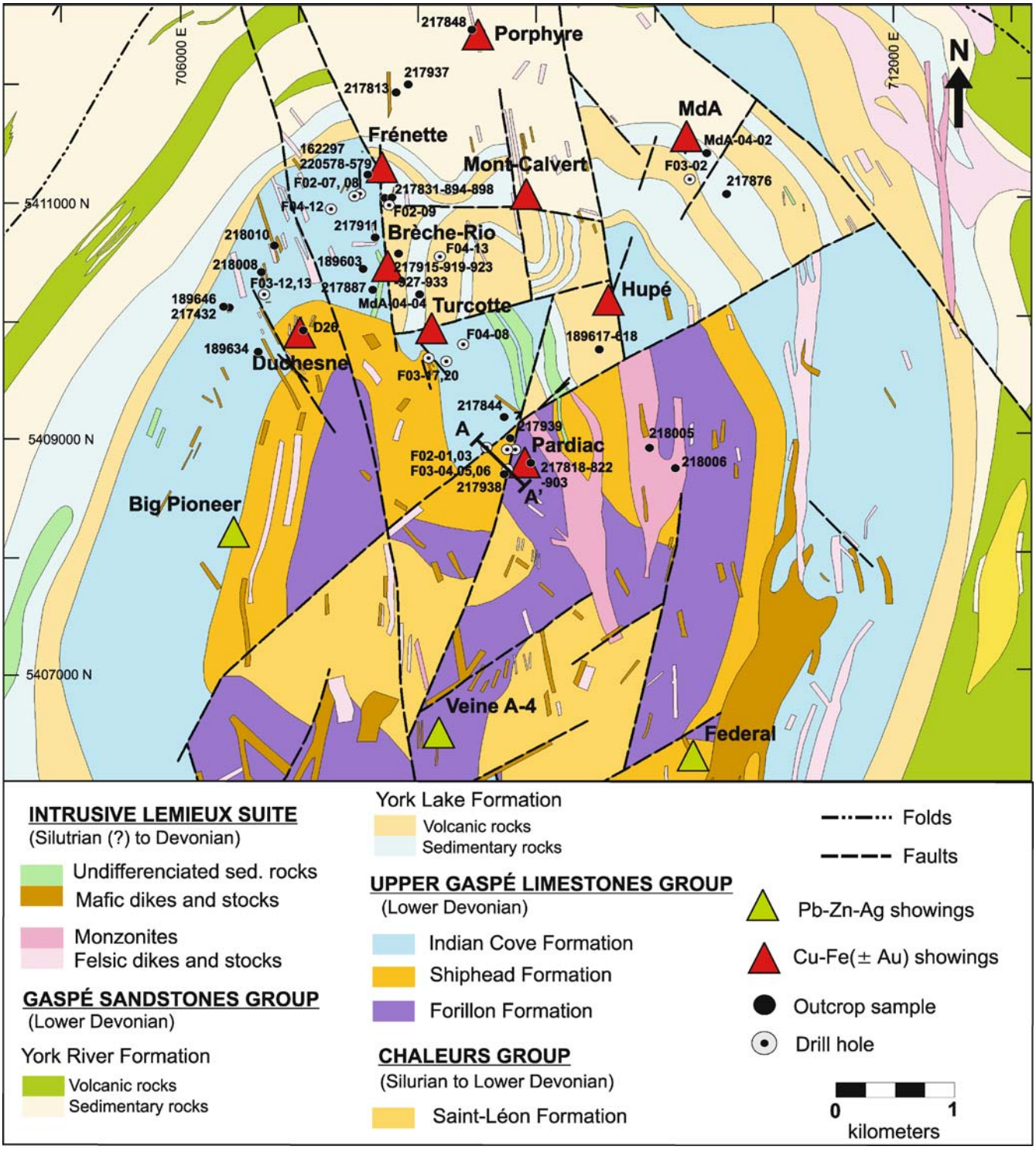

Fig. 2 Detailed geology of Cu–Fe (± Au) showings from the Mont-de-l'Aigle deposit, in the northern part of Dome Lemieux and the Pb–Zn–Ag showings in the southern part (modified from Pilote and Lachance 2003). Cross-section A–A′ is presented in Fig. 8

volcanic rocks assigned to the Chaleurs group. The Chaleurs group is overlain by the Upper Gaspé Limestones group that consists of shallow- to deep-water shelf carbonates deposited on a stable platform (Bourque et al. 1995). The Upper Gaspé Limestones group is overlain by the Gaspé Sandstones group that represents a gradually shallowing basin in an intra-arc extensional setting, and is accompanied by increasing bimodal volcanic activity (Bellehumeur and Valiquette 1993).

The Siluro–Devonian rocks of the Connecticut Valley-Gaspé Synclinorium are intruded by dikes and plutons spatially associated with Acadian faults. Bédard (1986) proposed that igneous rocks of Connecticut Valley-Gaspé Synclinorium formed in a within-plate anorogenic environment, perhaps in a transtensional back-arc basin, whereas Doyon (1992) suggested that they are typical of an extensional environment. Laurent and Dostal (1990) showed that these basalts are continental tholeiites with a transitional affinity related to within-plate extension. Whalen et al. (1994) proposed that plutonism occurred within a mainly extensional environment.

The Dome Lemieux is a 10 km-diameter subcircular anticline of Siluro–Devonian sedimentary and volcanic rocks located in the north central part of the Gaspé Peninsula (Figs. 1 and 2). This structure has been proposed to be the result of magma intrusion at depth (Gentile 1969; Bellehumeur and Valiquette 1993). Sedimentary rocks are cut by numerous mafic to felsic sills and dikes of the Lemieux Intrusive Suite that yielded an U−Pb zircon age of 398.3±0.8 Ma (Pilote and Lachance 2003). The mafic and felsic rocks of the Lemieux Intrusive Suite are along or near N−S, NW−SE, and NE−SW faults (Fig. 2). The Lemieux Intrusive Suite comprises fine-grained to porphyritic rocks that span a broad compositional range from tholeiitic to alkaline gabbros and diabases, subalkaline, peralkaline and alkaline granites, and felsites (Doyon 1992; Doyon and Dalpé 1993).

The McGerrigle plutonic complex, located northeast of the study area, yielded an U–Pb zircon age of 391.3± 3.4 Ma (Whalen et al. 1991). De Römer (1974) determined a K–Ar age of 371±11 Ma for Vallières-de-Saint-Réal Mountain and a 342±10 Ma age for Hog's Back Mountain. The Porphyry and Copper Mountain stocks at Mines Gaspé, Murdochville, yielded U−Pb zircon ages of 384.9± 2.5 and 384.8±2.8 Ma, respectively (Stephenson et al. 1998).

Metallogeny of the northern Gaspé Peninsula

The northern Gaspé Peninsula contains Cu-skarns, Pb−Zn−Ag epithermal veins, Cu-replacement mantos and Cu−Mo porphyry mineralization. Several Ni−Cr showings are associated with ultramafic units of the Ruisseau Isabelle Mélange along the Shickshock-Sud fault (Fig. 1; Gosselin 2000). Mines Gaspé (Fig. 1) comprises the Copper Mountain Cu−Mo porphyry and Needle Mountain Cu-skarn deposits that together produced approximately 124 Mt with an average grade of 0.64% Cu with recoverable molybdenum, silver, bismuth, selenium, tellurium, and gold (Swinden and Dunsworth 1995). In 1994, the Porphyry Mountain Cu–Mo porphyry deposit was defined with a tonnage of 206 Mt, averaging 0.73% Cu and 0.08% Mo (Stephenson et al. 1998). The Sullipek deposit, located 30 km southwest of Mines Gaspé (Fig. 1), is a Fe–Au–Cu skarn formed from pure marbles of the uppermost Silurian West Point Formation that was intruded by dacitic porphyries overprinted by strong potassic and sodic alteration (Wares 1986). The Sullipek fault system controls skarn occurrences (Wares 1986) that contain 0.5 Mt grading 1.4% Cu, 0.025% MoS_2, and 7 g/t Ag (Wares 1983).

The Federal Mine, in the southern part of Dome Lemieux, comprises a series of subvertical crustiform quartz–carbonate–sphalerite–galena veins that are spatially associated with felsic dikes. The veins were interpreted to be examples of epithermal-type deposits related to felsic volcanism (Pilote 2005). These veins are rich in amethyst and contain alternating bands of quartz and dolomite (Stevens 1986). The vein system has produced about 0.6 Mt grading 3.95% Zn and 1.31% Pb (Swinden and Dunsworth 1995). According to Stevens (1986), the hydrothermal system was driven by deep-seated intrusions, the upper parts of which are exposed as rhyolite porphyry apophyses. He identified hematite–pyrite–chalcopyrite veins that displayed a strong spatial association with a zone of rhyolite porphyry intrusions in the northern part of the Dome Lemieux. Stevens (1986) showed that the temperature of mineral deposition ranged from 50 to 460°C for quartz. Quartz–hematite–pyrite–chalcopyrite veins inclusions fluids are interpreted to have boiled intermittently between 295 and 460°C in veins and fractured porphyries and have salinities ranging from 0 to 26 wt% NaCl equivalent.

Analytical methods

Whole rock major and trace elements from 50 least altered to altered igneous rocks (type 1 to type 4) and 33 samples of sedimentary rocks were determined by lithium metaborate/tetraborate fusion inductively coupled plasma (ICP) and by inductively coupled plasma-mass spectrometry (ICP-MS) at Activation Laboratories, Ancaster, Ontario. Chlorite, feldspar, dolomite, calcite, hematite, and sulfide mineral composition were determined using the 5 WDS CAMECA SX-100 electron microprobe at Université Laval, Québec, Canada. Analytical conditions were 15 kV and 20 nA with counting times of 20 s on peak and 10 s on background. A combination of natural and synthetic standards was used.

Sulfur isotope analyses of pyrite and chalcopyrite separates were performed by the G.G. Hatch Isotope Laboratory, University of Ottawa, Canada. The sulfur isotope composition was determined by continuous flow isotope ratio mass spectrometry (CF-IRMS). SO_2 was produced by flash combustion with vanadium pentoxide at 1,800°C in an elemental analyzer, followed by gas

chromatography before injection into a Finnigan MAT Delta^{+} mass spectrometer. Quartz and hematite were reacted with BrF_5 according to the method of Clayton and Mayeda (1963) at the Stable Isotope Laboratory of Université Laval. For each analysis, about 20 mg of sulfide, quartz, and hematite concentrates were prepared under a binocular microscope. Isotope ratios are reported in δ-notation relative to *V*-SMOW (oxygen) and *V*-CDT (sulfur) with a precision better than ±0.2‰.

Local geology

The lowest stratigraphic unit of the Dome Lemieux anticline is the upper part of the terrigenous Saint-Léon Formation at the top of the Chaleurs group. The St-Léon Formation crops out in the south central part of the anticline and is dominated by black mudstone and claystone, calcareous quartz sandstone, and siltstone (Pilote and Lachance 2003). At the level of exposure, rocks of the Saint-Léon Formation display subgreenschist metamorphism but they have been metamorphosed to hornfels and garnet-clinopyroxene skarn above granitic intrusions cut by diamond drill holes at depths greater than 500 m (Bellehumeur and Valiquette 1993). The Saint-Léon Formation is in gradational contact with the overlying Forillon Formation or in fault contact with the Forillon, Shiphead, and Indian Cove formations of the Upper Gaspé Limestones group (Fig. 2). The Forillon Formation consists of a sequence of dolomitic and siliceous calcilutite or limy mudstone, whereas the overlying Shiphead Formation is characterized by bedded siliceous and dolomitic limestone and mudstone, with minor calcarenite, sandstone, and bentonite beds (Malo and Bourque 1993; Bourque et al. 1995). The Shiphead Formation is overlain by the Indian Cove Formation that consists of cherty to siliceous or silty calcilutite. Minor mafic and felsic volcanic rocks occur within these formations.

The overlying Gaspé Sandstones group comprises the York Lake and York River formations. The York Lake Formation is composed of siliceous calcilutite with minor quartz arenite and medium-grained feldspathic wacke (Malo and Bourque 1993; Bourque et al. 1995). The overlying York River Formation is composed of a lower unit of mudstone–siltstone–sandstone with a few calcarenite beds and an upper unit of sandstone interlayered with a 100-m thick bimodal volcanic sequence. This sequence is composed of basaltic flows and mafic pyroclastic rocks, overlain by rhyolitic flows and felsic pyroclastic rocks that are capped by rhyolitic flows (Doyon 1988; Bourque et al.

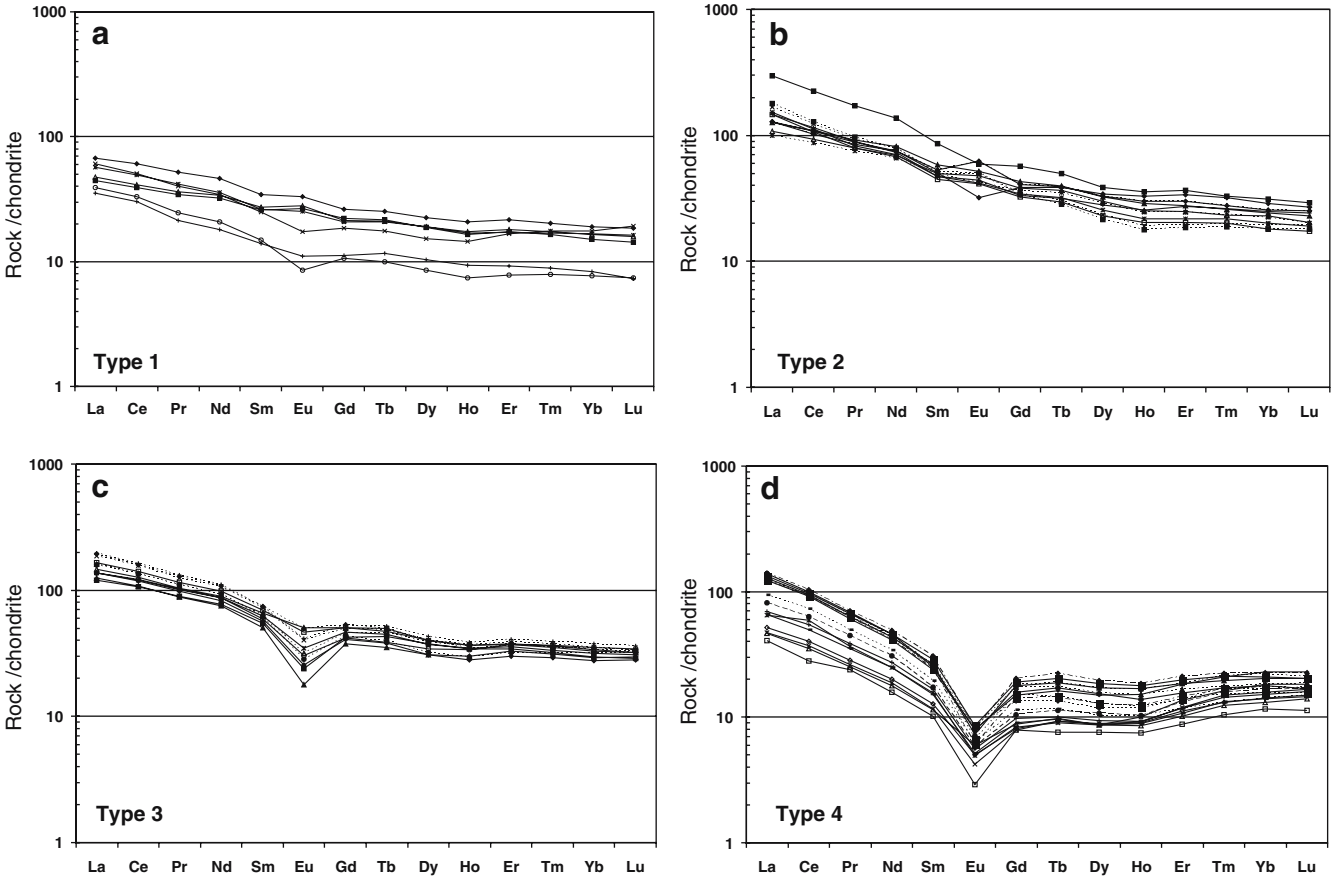

Fig. 3 Rare earth element composition of intrusions from the Mont-de-l'Aigle deposit normalized to chondrite values from McDonough and Sun (1995). Sample numbers refer to Table 1. **a** Type 1. **b** Type 2. **c** Type 3. **d** Type 4

1995). Rhyolite occurs mainly at Lyall Mountain, to the east of Dome Lemieux, at Tuzo and Squaw Cap Mountains, to the west of Dome Lemieux or form scattered occurrences near its center.

Intrusions

Rocks of the Lemieux Intrusive Suite from the Mont-de-l'Aigle deposit comprise mafic and felsic dikes. Four populations of igneous rocks are recognized on the basis of chondrite-normalized Rare Earth Elements (REE) patterns (Fig. 3), and trace element geochemistry: three types of mafic dikes (types 1–3) and one type of felsic

Table 1 Representative major and trace-element composition of intrusions from the Mont-de-l'Aigle deposit, Gaspé Peninsula, Quebec

Sample Dyke Type	Altered				Least-altered			
DDH	218873	218804	218832	218889	218867	218869	218862	218850
	1	2	3	4	1	2	3	4
	F02-09	F02-07	F02-07	F03-13	F02-03	F02-08	F03-12	F03-17
SiO_2 (wt%)	49.42	45.74	51.48	76.59	44.41	41.51	49.17	74.56
Al_2O_3	16.63	12.74	15.67	10.25	15.10	14.38	16.01	11.83
TiO_2	1.84	1.82	2.80	0.14	1.54	2.92	2.35	0.15
Fe_2O_3[a]	14.85	18.89	11.97	4.25	13.48	13.99	15.14	2.31
MnO	0.18	0.24	0.17	0.07	0.26	0.24	0.20	0.06
MgO	4.47	10.70	4.47	1.71	8.58	6.53	6.04	1.25
CaO	0.85	0.77	1.14	0.16	5.34	7.47	0.92	0.30
Na_2O	5.64	0.75	1.64	0.13	0.98	1.90	3.75	1.92
K_2O	0.09	0.07	5.95	4.64	3.44	1.68	1.03	6.08
P_2O_5	0.27	0.40	0.65	0.03	0.20	0.57	0.61	0.03
LOI	4.56	6.64	3.57	2.17	5.78	7.89	4.29	1.20
Total	98.51	98.75	98.80	100.15	99.10	99.07	99.50	99.68
Ba (ppm)	21	32	2,052	1,551	2,018	560	291	2,710
Co	29	52	22	7	30	31	17	3
Cu	ND	ND	14	ND	52	45	ND	ND
Nb	29	18	22	16	8	24	20	18
Ni	25	50	ND	ND	98	56	ND	ND
Rb	ND	7	127	106	82	29	17	114
Sr	87	31	164	91	343	361	114	110
Th	7	4	5	17	1	2	5	18
V	237	212	189	12	211	325	222	9
W	10	11	4	ND	ND	ND	3	ND
Y	19	29	46	15	24	39	48	30
Zn	49	80	74	ND	46	62	65	ND
Zr	182	178	325	101	116	276	317	114
La	14.4	34.6	44.2	16.3	10.5	29.9	28.4	33.4
Ce	30.9	65.2	95.5	33.6	23.9	66.7	65.6	63.9
Pr	3.7	7.4	11.6	3.6	3.2	8.5	8.3	6.6
Nd	15.7	30.7	48.4	12.5	14.7	37.0	35.4	22.4
Sm	3.7	6.6	10.7	2.4	3.8	8.6	8.1	4.5
Eu	0.9	2.3	2.3	0.3	1.4	2.9	1.3	0.4
Gd	3.7	6.5	9.9	1.9	4.4	8.6	8.4	4.1
Tb	0.6	1.1	1.7	0.4	0.8	1.4	1.5	0.8
Dy	3.7	5.7	9.9	2.3	4.6	8.0	9.2	4.8
Ho	0.8	1.1	2.0	0.5	0.9	1.6	1.9	1.0
Er	2.6	3.2	6.2	1.9	2.8	4.4	5.5	3.4
Tm	0.4	0.5	0.9	0.3	0.4	0.6	0.8	0.5
Yb	2.8	2.9	5.7	2.4	2.4	3.9	4.8	3.6
Lu	0.5	0.4	0.8	0.4	0.4	0.6	0.7	0.5
ΣREE	84.8	168.3	249.9	78.9	74.4	182.8	180	150

ND Not detected
[a]Total Fe as Fe_2O_3

dikes (type 4). Representative chemical composition of each dike type is provided in Table 1, whereas the whole dataset is in Table 10 in Appendix. The mafic dikes are fine-grained, gray to green (due to high chlorite concentration) in a groundmass of quartz, and orthoclase with minor albite. Porphyritic textures are developed locally with up to 10% albite or orthoclase phenocrysts (0.1–2 mm). The accessory minerals include rutile, fluoroapatite, and minor zircon. Fluoroapatite forms idiomorphic grains (up to 70 μm) disseminated in the groundmass of mafic dikes. Mafic dikes contain up to 5% disseminated pyrite and are cut by veins and veinlets of quartz, hematite, dolomite, and pyrite.

Felsic dikes are porphyritic with up to 15% albite or orthoclase phenocrysts (0.05–1.5 mm) in fine-grained to aphanitic pale gray to pink groundmass, composed of quartz and accessory rutile. Rare chlorite is found in the groundmass of felsic dikes or replaces albite and orthoclase phenocrysts. Felsic dikes are cut by orthoclase, quartz, and hematite veins and veinlets. The absence of recognizable cross cutting relationship among the four intrusion types precludes determination of the relative timing of emplacement.

On the Zr/TiO_2 vs Nb/Y discrimination diagram (Fig. 4a), mafic dikes span a broad compositional range from dacite to alkaline basalt with 28 to 56 wt% SiO_2 (Fig. 4b,c; Table 1; Table 10 in Appendix). Figure 4b indicates that mafic dikes are alkaline to subalkaline. However, mafic dikes plot mostly in the transitional field (Zr/Y=4–7), although some dikes plot in the calc-alkaline field (Fig. 4d). Type 1 dikes have concentration in Y (10–30 ppm) and Zr (60–145 ppm), lower than types 2 and 3 dikes that are enriched in Y (20–50 ppm) and Zr (140–350 ppm) (Fig. 4d; Table 1; Table 10 in Appendix). Type 1 dikes show slight positive to negative europium anomalies (Eu_n/Eu_n*=0.7–1.2) and have the least fractionated REE pattern with average La_n/Lu_n=3.8 and La_n/Sm_n=2.2 (Fig. 3a; Table 1; Table 10 in Appendix). Type 2 dikes are fractionated with average La_n/Lu_n=6.9 and La_n/Sm_n=2.0, and display small negative or positive europium anomalies (Eu_n/Eu_n*=0.7−1.3; Fig. 3b; Table 1; Table 10 in Appendix). Type 3 dikes are slightly fractionated (La_n/

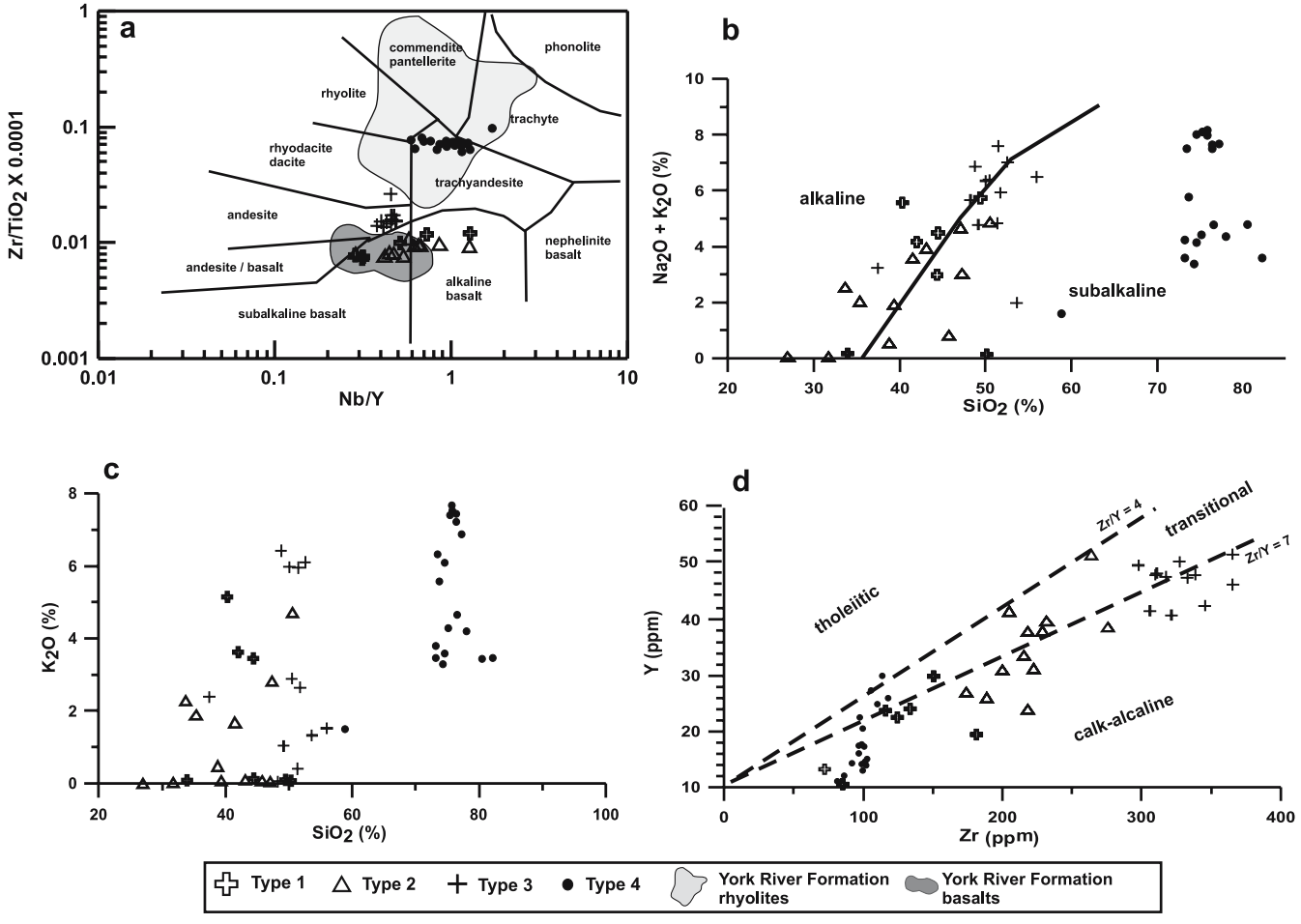

Fig. 4 Geochemistry of the Siluro–Devonian intrusions of the Mont-de-l'Aigle deposit. **a** Zr/TiO_2 vs Nb/Y diagram where field boundaries are from Winchester and Floyd (1977). Intrusions from the Mont-de-l'Aigle deposit are compared to the fields of rhyolite and basalt from the York River Formation (Doyon and Valiquette 1991). **b** SiO_2 vs $Na_2O + K_2O$ diagram of Irvine and Baragar (1971). **c** K_2O vs SiO_2 diagram. **d** Magmatic affinity using the Y vs Zr diagram of Barrett and MacLean (1994)

Lu_n=4.8) with a negative europium anomaly (Eu_n/Eu_n*=0.4–0.9; Fig. 3c; Table 1; Table 10 in Appendix).

Type 4 felsic dikes range in composition from trachyandesite to rhyodacite/dacite (Fig. 4a) with SiO_2 concentration ranging from 58 to 83 wt% (Fig. 4b,c), whereas K_2O ranges from 3.5 to 8 wt% (Fig. 4c; Table 1; Table 10 in Appendix). Figure 4b indicates that felsic dikes are subalkaline whereas, Fig. 4d shows that they plot mostly in the transitional field, although some dikes plot in the tholeiitic field. Type 4 dikes have concentration in Y (10–32 ppm) and Zr (80–110 ppm), lower than types 2 and 3 dikes (Fig. 4d; Table 1; Table 10 in Appendix). Type 4 dikes display a fractionated pattern enriched in light rare earth elements (LREE) with average La_n/Sm_n=4.7 and La_n/Lu_n=5.9 (Fig. 3d, Table 1; Table 10 in Appendix), but also display a small heavy REE enrichment indicated by average Gd_n/Lu_n=0.8. Type 4 dikes have a larger negative europium anomaly (Eu_n/Eu_n*=0.3–0.6) than types 2 and 3 mafic dikes (Fig. 3d).

Tectonic setting

The Y vs Th diagram (Fig. 5a) shows the relationship between differentiation and contamination for incompatible elements (Doyon and Berger 1997). Y is used as an immobile contamination index, whereas Th is used as differentiation index. Figure 5a shows that type 1 dikes have the most primitive composition (ΣREE=84.8 ppm; Table 1), but display evidence of crustal contamination with Y content less than 25 ppm (Fig. 5a). Types 2 and 3 dikes plot along a differentiation trend from type 1 dikes and have a signature similar to that of the mafic dikes at Mines Gaspé (Doyon and Berger 1997). Differentiation by

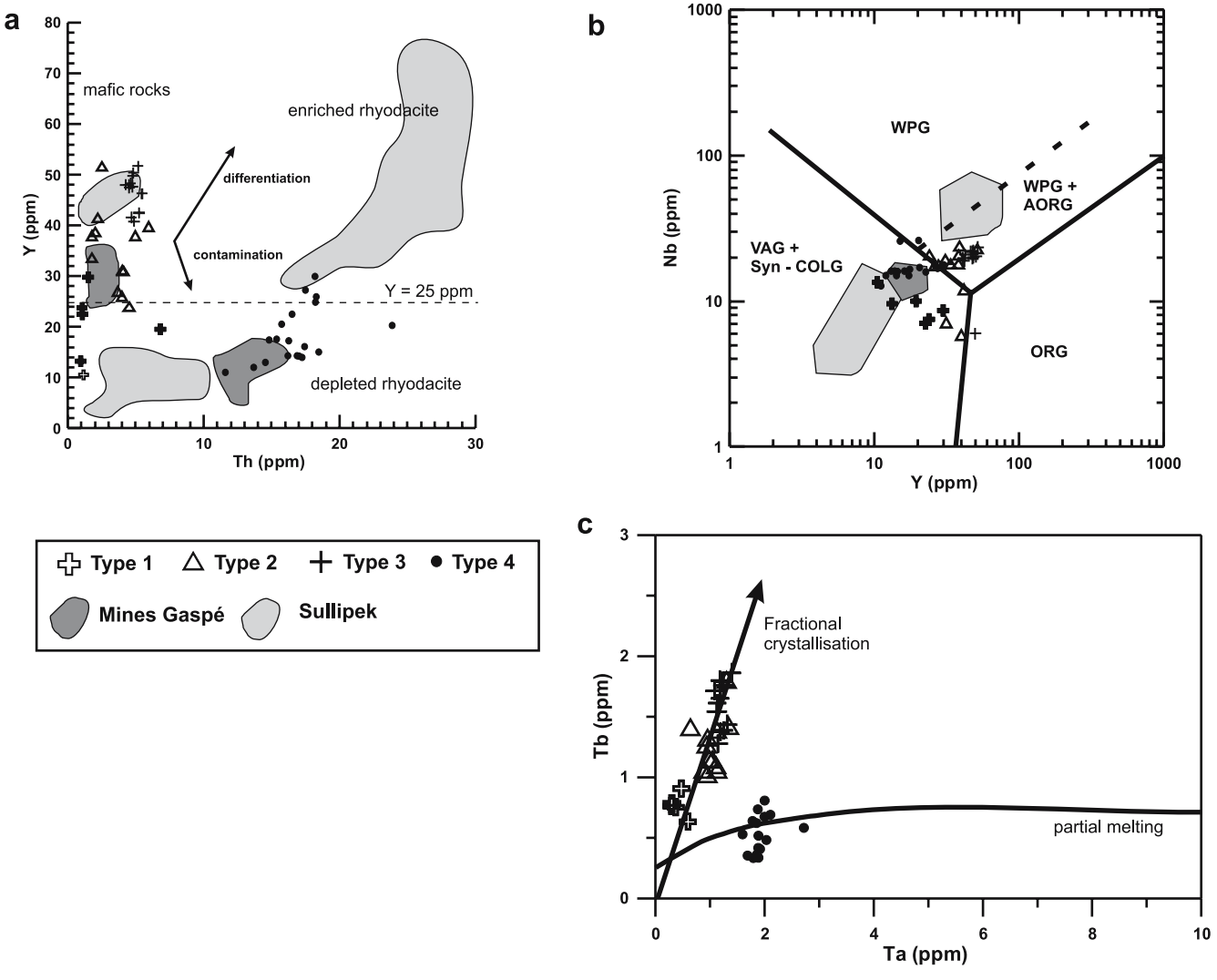

Fig. 5 Intrusions from the Mont-de-l'Aigle deposit compared to mafic and felsic intrusions from Mines Gaspé and Sullipek. **a** Y vs Th diagram illustrating the relation between contamination and differentiation trends (Doyon and Berger 1997). **b** Tb vs Ta diagram of Treuil and Varet (1973) illustrating that types 1–3 dikes are derived from fractional crystallization of a common magma, whereas felsic dikes are derived by partial melting. **c** Nb vs Y discriminant diagram for tectonic affinity. Field boundaries are from Pearce et al. (1984). *ORG* Ocean ridge granites, *VAG* volcanic arc granites, *WPG* within plate granites, *syn-COLG* syn-collision granites, *AORG* anorogenic granites

fractional crystallization is indicated by covariation of Tb and Ta (Fig. 5b). Types 2 and 3 dikes are characterized by a within-plate affinity with two samples having volcanic arc affinity (Fig. 5c). Figure 5a shows that type 4 dikes have Y−Th composition similar to depleted rhyodacite and felsic intrusions associated with Cu-porphyry mineralization at Mines Gaspé. Felsic dikes show increased Y that could be a consequence of differentiation (Fig. 5a). Type 4 dikes have different Tb−Ta that indicates derivation by partial melting instead of differentiation from the mafic dikes (Fig. 5b). Type 1 dikes and type 4 dikes have a volcanic arc affinity similar to Sullipek mafic and Mines Gaspé felsic rocks associated with Cu-porphyry and skarn mineralization (Fig. 5c).

Cu–Fe (± Au) mineralization

The Mont-de-l'Aigle deposit is comprised of nine Cu–Fe (± Au) showings in the northern part of Dome Lemieux (Fig. 2). The mineralization comprises veins, stockworks, breccias, and disseminated oxides and sulfides. Stratigraphic position of each showing is summarized in Fig. 7. Hematite veins cut hornfels (Fig. 6a) and skarns in the Saint-Léon Formation at depth (Bellehumeur and Valiquette 1993), epithermal mineralization typical of the southern part of the dome, and mafic and felsic dikes of the Lemieux Intrusive Suite (Fig. 6b) that indicate a maximum age of 398.3±0.8 Ma for mineralization.

The Pardiac showing lies along a NNE–SSW fault (Fig. 2) where a mafic dike is cut by quartz–hematite–pyrite veins in the northern part of the showing. Mineralization is hosted by stockworks and breccias over a strike length of 175 m with a thickness ranging from 10 to 40 m (Figs. 6f, 7, and 8). A NW–SE cross-section of the Pardiac showing shows the spatial relationship among mafic intrusions, breccia zones, and copper mineralization (Fig. 8). The Pardiac showing (Fig. 2) is hosted by black and green limestone of the Forillon and Shiphead formations and is characterized by quartz, hematite, pyrite,

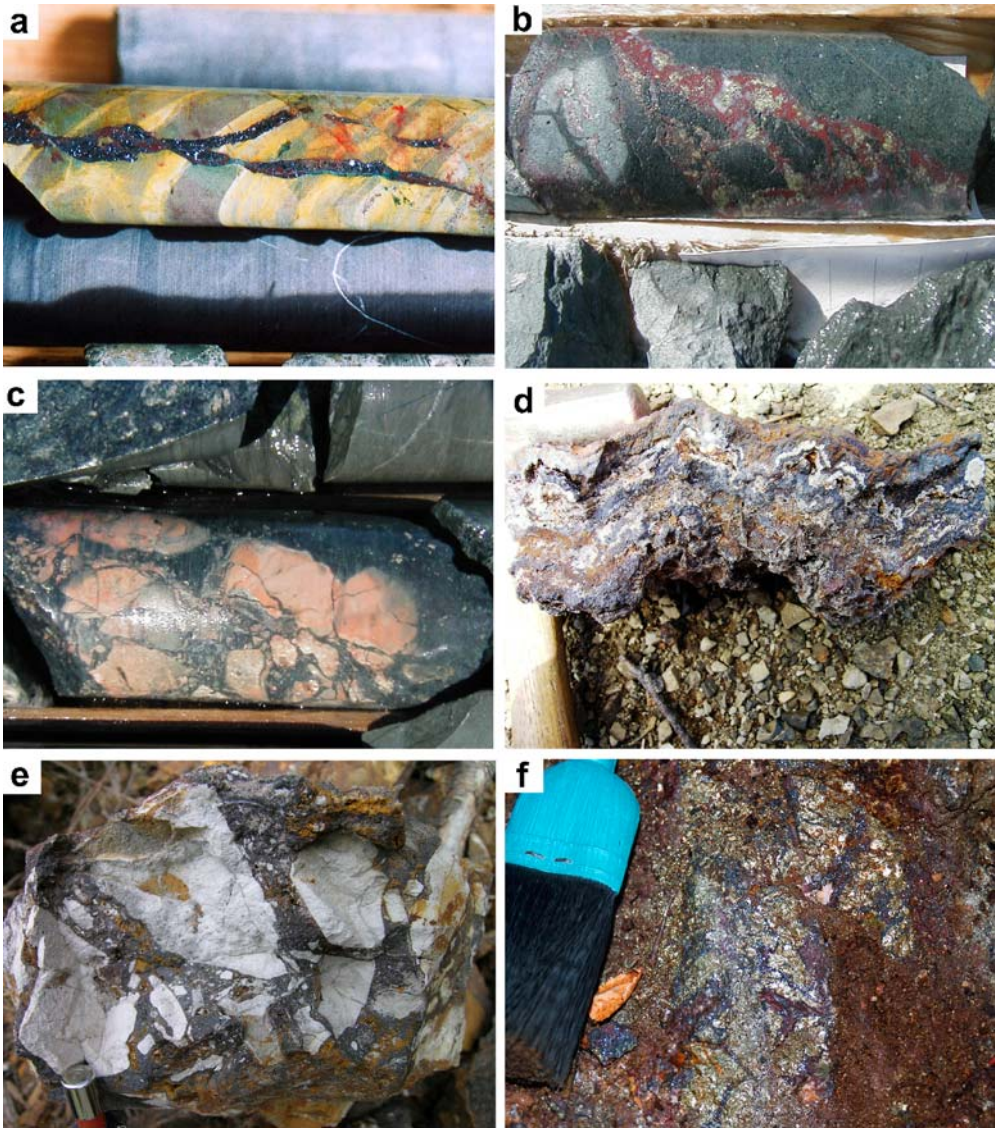

Fig. 6 Photographs of alteration and mineralization. **a** Hematite vein cutting hornfels from the Pardiac showing (core is 36.5 mm in diameter). **b** Hematite–chalcopyrite–quartz veins cutting a mafic dike from the Frenette showing (core is 36.5 mm in diameter). **c** Breccia with potassic altered fragments of mafic intrusions in chlorite-rich matrix from the Pardiac showing (core is 36.5 mm in diameter). **d** Crustiform vein from the Turcotte showing displaying alternating bands of magnetite, hematite, and dolomite. **e** Hematite-rich breccia matrix containing argillic altered fragments of sedimentary rocks, MdA showing. **f** Typical outcrop from the Pardiac showing with massive chalcopyrite, pyrite, hematite cemented by quartz

and chalcopyrite veins with local magnetite. Southeast of the fault (Fig. 8), mineralization is hosted by brecciated limestone and mafic dikes. Hematite, magnetite, and quartz commonly occur as crustiform veins, whereas pyrite and chalcopyrite occur as disseminations (5–20%) in veins, stockworks, breccia cement, and host rocks. Pyrite and chalcopyrite also form massive veins and veinlets, whereas pyrite-rich fragments occur in breccias. Drusy quartz coats small cavities at the core of veins and breccias. Two types of breccias are recognized at the Pardiac showing: (1) mineralized breccias containing subrounded to subangular hostrock fragments (1–3 cm) are cemented by hematite with less than 50% of quartz, and (2) barren breccias with jigsaw texture and angular fragments containing more than 50% quartz (Bernard et al. 2005). Grades up to 1.0% Cu over 10.5 m and 91 ppb Au over 3.5 m (Table 2) have been returned from drill holes. The host limestone is strongly silicified, chloritized, and decalcified. Breccias in mafic dikes contain potassic-altered fragments cemented by chlorite (Fig. 6c).

The Turcotte showing has a strike length of 400 m with a thickness ranging from 20 to 30 m. Mineralization is spatially related to a minor NW–SE fault. A NW–SE mafic dike is cut by hematite, pyrite, and quartz veins (Figs. 2 and 7). The Turcotte showing is hosted by chloritized and silicified limestone, mudstone, and quartzite of the Shiphead and Indian Cove formations (Fig. 2). Mineralization is characterized by hematite, magnetite, quartz, pyrite, and chalcopyrite in veins and stockworks with local breccias (Fig. 7). Mineralization occurs as zoned crustiform veins of hematite, magnetite and quartz with a late stage of drusy quartz (Fig. 6d). Some breccias contain epithermal-style amethyst and pyrite-rich fragments. The best drill intersection grades 0.16% Cu over 18.5 m (Table 2). A chlorite, hematite, and pyrite-rich quartzite bed of the Indian Cove Formation may represent stratabound manto mineralization, and is cut by a stockwork cemented by quartz, pyrite, and chalcopyrite.

The Brèche-Rio showing is a 200-m long N−S body of breccia and stockwork located at the N−S fault contact between the Indian Cove and the York Lake formations

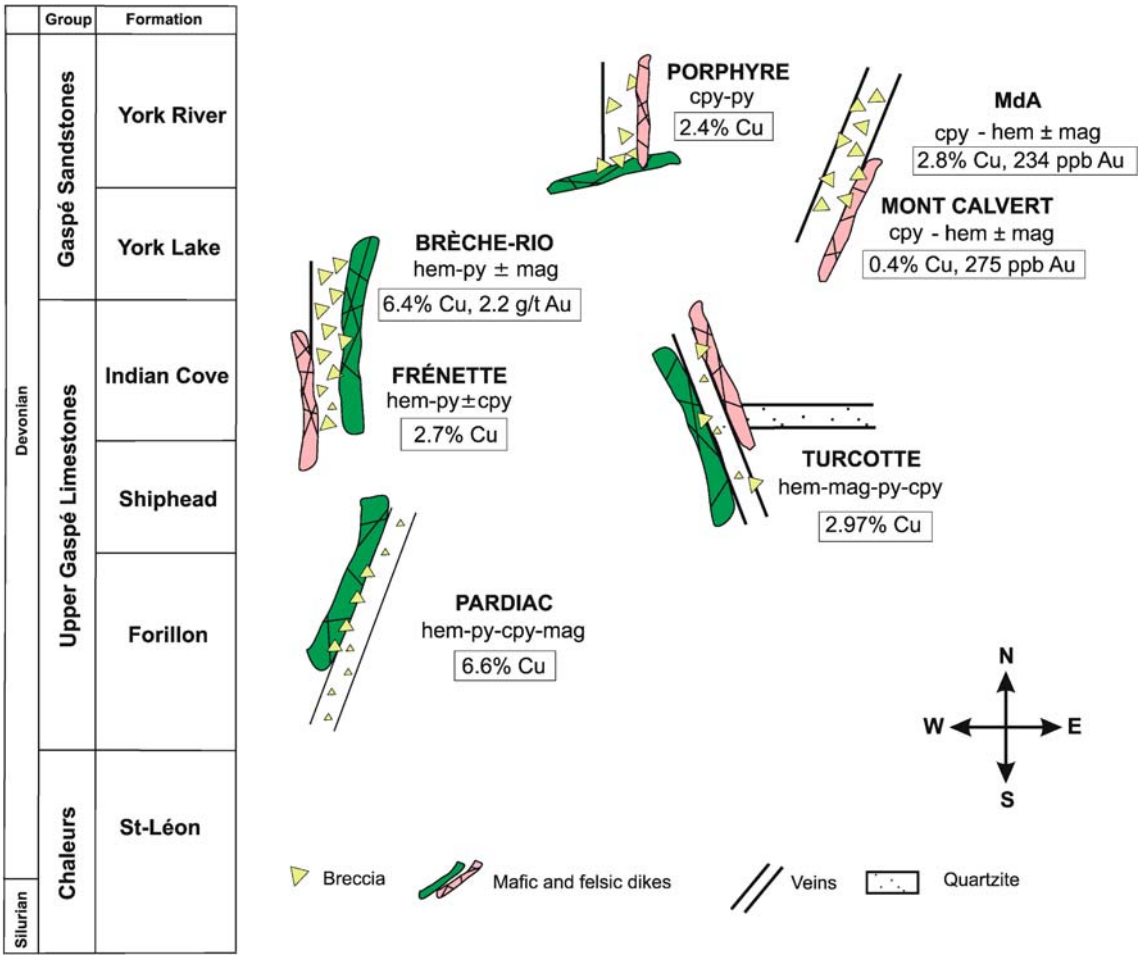

Fig. 7 Stratigraphic positions of Cu–Fe (± Au) showings from the Mont-de-l'Aigle deposit associated with faults and/or intrusions. Cu–Fe (± Au) breccias dominate mineralization in the Gaspé Sandstones group. Mineralogy and highest copper and gold grades from grab samples for each showing is indicated. Quartzite represents stratabound mineralization at the Turcotte showing. *Cpy* Chalcopyrite; *Hem* hematite; *Mag* magnetite; *Py* pyrite

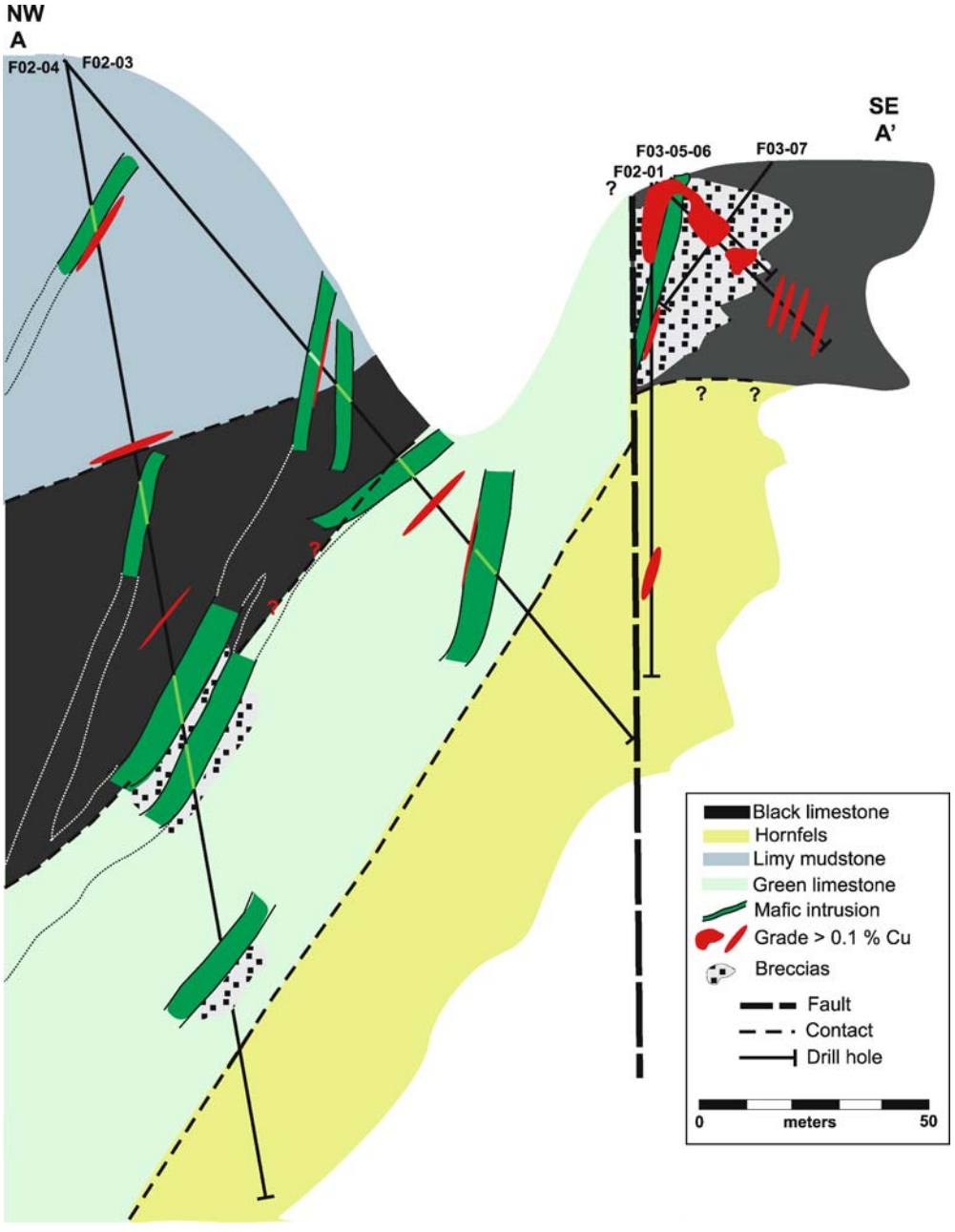

Fig. 8 Cross-section A–A′ through the Pardiac showing (Fig. 2), reveals the close spatial relationship among mafic dikes, breccias, and high-copper grade (>0.1% Cu). No vertical exaggeration

(Fig. 2). Breccias contain Siluro–Devonian sedimentary rock fragments with well-developed chlorite and silica alteration, and are cemented by quartz, pyrite, and specular hematite (Fig. 7; Bernard et al. 2005). The best drill hole intersected 0.15% Cu and 117 ppm Co over 45 m (Table 2) and a grab sample in a quartz–hematite breccia has returned 2.2 g/t Au (217887; Fig. 2). One type of breccia is characterized by white clay-altered fragments cemented by massive hematite (Fig. 6e).

The Frenette showing is about 75 m long with a thickness ranging from 10 to 40 m (Fig. 2). The Frenette showing comprises pyrite–hematite–magnetite ± chalcopyrite veins, stockworks, and breccias cutting chloritized and silicified limestone and siltstone of the Indian Cove Formation and N–S mafic and felsic dikes of the Lemieux Intrusive Suite (Figs. 2 and 7). Veins and stockworks contain up to 10% fragments of chloritized sedimentary rocks in a cement of drusy quartz, pyrite, and hematite. Breccias have massive hematite-rich matrix cut by late about 15 cm width N–S and NW–SE barite veins. The best drill intersection in this showing grades 0.11% Cu over 9.3 m (Table 2). The mafic dikes display strong chlorite alteration, whereas felsic dikes are characterized by pink potassic alteration.

The MdA showing is located along a NE−SW minor fault (Fig. 2). This showing (Figs. 2 and 7) is composed of hematite−quartz cemented breccias with fragments of altered Siluro–Devonian sedimentary rocks (Fig. 6e) and quartz–chalcopyrite ± hematite–magnetite stockworks hosted by limestone and sandstone of the York Lake and

Table 2 Base- and precious-metal assay data of selected drill holes from the Mont-de-l'Aigle deposit, Gaspé Peninsula, Quebec

Showing	DDH	Dip	Length (m)	Cu (%)	Au (ppb)	Zn (ppm)	Pb (ppm)	Co (ppm)
Pardiac	F02-01	90	15.0	0.17	55	76	34	–
	F02-01	90	3.5	0.16	91	69	51	–
	F02-01	90	10.5	1.00	–	90	7	–
	F03-04	45	5.9	0.56	20	70	25	75
	F03-05	45	28.0	0.21	18	84	19	56
	F03-06	45	49.2	0.14	24	98	10	44
	F03-06	45	2.25	–	45	–	–	–
Turcotte	F03-17	45	18.5	0.16	7	98	6	41
	F03-20	45	49.3	0.12	8	68	9	34
Frenette	F02-07	45	9.3	0.11	–	85	–	–
Brèche-Rio	F04-12	90	45.0	0.15	32	71	8	117
	F04-13	80	10.1	0.13	59	194	13	55
MdA	F03-02	55	15.5	0.25	100	–	–	–

York River formations. The best drill intersection grades 0.25% Cu and 0.1 g/t Au over 15.5 m (Table 2).

The Porphyre showing is hosted by York River Formation chloritized sandstone and consists of quartz–chalcopyrite–pyrite veins, stockworks, and breccias along the contacts with E–W chlorite-altered mafic and N–S potassic-altered felsic dikes (Figs. 2 and 7). Veins of massive sulfide containing parallel bands of pyrite and chalcopyrite occur locally but no iron oxides are known. The breccias intrusive and sedimentary rock fragments are chlorite-altered and cemented by quartz with disseminated chalcopyrite and pyrite.

Mineralogy and paragenetic sequence

The mineral assemblage of the Mont-de-l'Aigle deposit consists of hematite (≤40%), pyrite, chalcopyrite, and magnetite (≤15%) with quartz, dolomite, and chlorite as gangue minerals. The generalized paragenetic sequence is divided into three main stages (Fig. 9): (1) early pervasive sodic, potassic, chlorite, and silica alteration, (2) hematite, quartz, pyrite, chalcopyrite, and magnetite cementing veins, stockworks and breccias, and (3) late dolomite ± hematite and barite veins and veinlets.

Pyrite occurs as euhedral to subhedral grains (10–20 μm) disseminated in host rocks or aggregates (2 mm–1 cm) in veins, stockworks, and breccias, where pyrite is interstitial to quartz, dolomite, and chlorite. Pyrite has low As (0.01−0.40 wt%) and Co contents (0.01–0.18 wt%; Table 3). Pyrite is cut by specular hematite (Fig. 10a) and is overgrown by chalcopyrite (Fig. 10b). Chalcopyrite is characterized by anhedral to subhedral disseminated grains (25–200 μm) interstitial to quartz and dolomite in veins, stockwork, or breccias. Chalcopyrite overgrows hematite needles and pyrite (Figs. 9 and 10b,d). Well-formed late drusy quartz cores veins, stockworks, and breccias.

Hematite occurs as euhedral grains ranging from 10 to 50 μm that exhibit tabular habit (specular) and is associated with quartz or dolomite in veins. A first generation of abundant hematite is associated with the first stage of mineralization; whereas, the second stage hematite occurs with late dolomite veins (Fig. 9). Massive hematite forms the cement of breccias at the Brèche-Rio (Fig. 6e) and the MdA showings. Hematite replacement by pseudomorphic magnetite (mushketovite) is common in veins and breccias

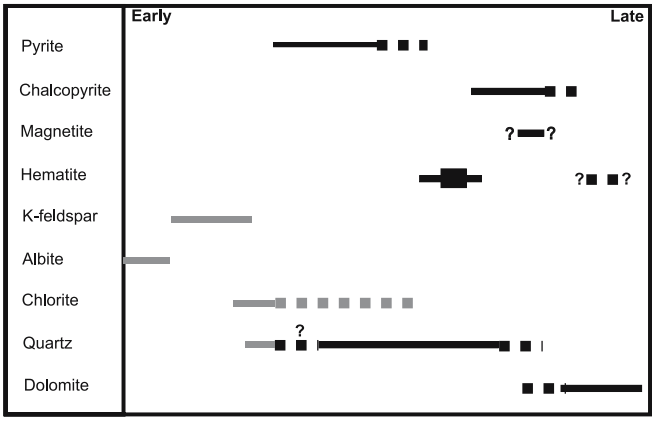

Fig. 9 Paragenetic sequence for the Mont-de-l'Aigle deposit

Table 3 Representative microprobe composition of pyrite from the Mont-de-l'Aigle deposit, Gaspé Peninsula, Quebec

Sample no.	217848	220515	217818	220514
Analysis no.	Py 1	Py 1	Py 1	Py 3
Cu (wt%)	ND	ND	ND	ND
Fe	47.94	48.37	48.15	47.89
Co	ND	ND	ND	ND
Ni	ND	0.01	ND	ND
S	51.56	51.36	52.36	52.07
As	0.20	ND	ND	0.07
Total	99.87	99.76	100.62	100.02

ND Not detected

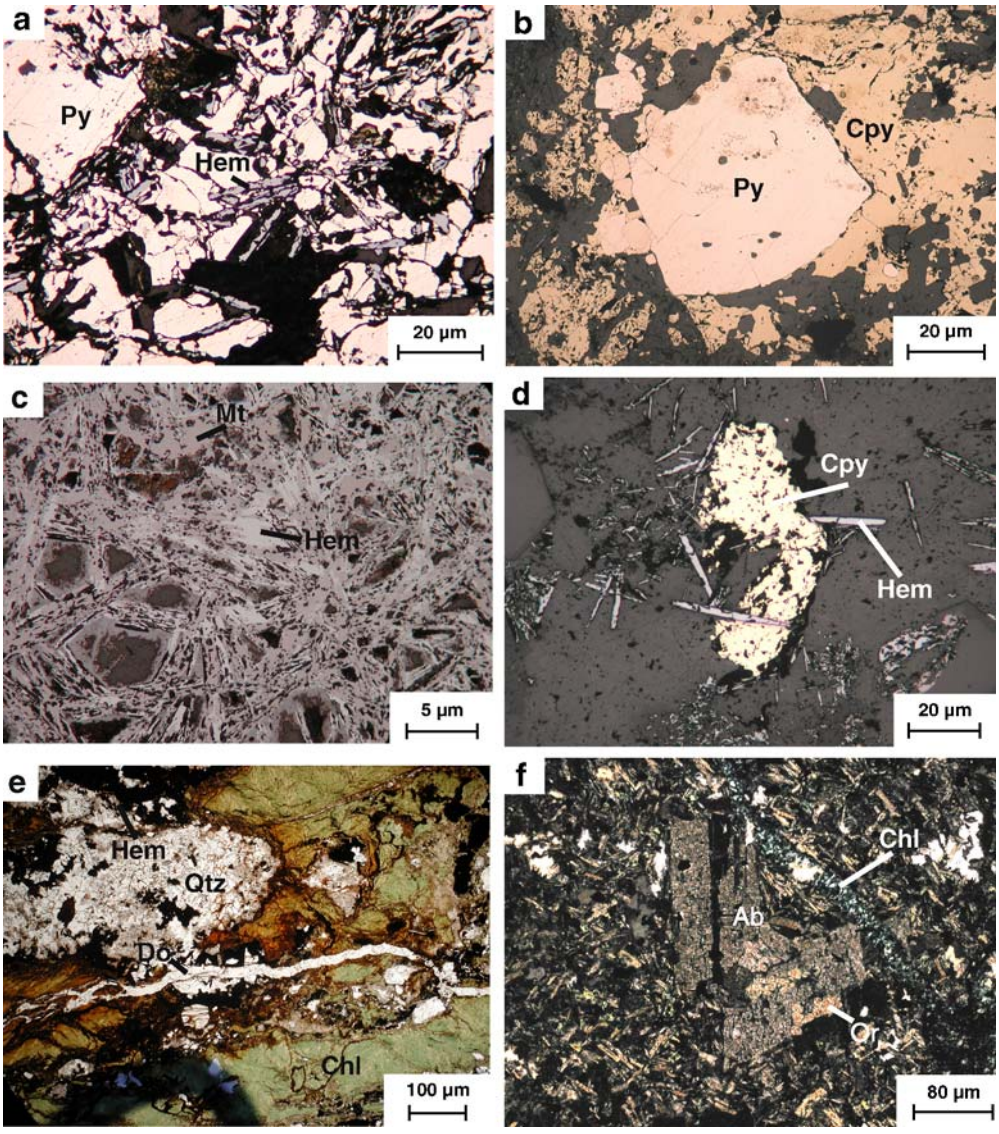

Fig. 10 Photomicrographs of mineralization and alteration textures. **a** Pyrite cut by specular hematite (reflected plane polarized light). **b** Chalcopyrite overgrowing pyrite (reflected plane polarized light). **c** Pseudomorphic replacement of hematite by magnetite (mushketovite; reflected plane polarized light). **d** Chalcopyrite overgrowing early specular hematite (reflected plane polarized light). **e** Late dolomite veinlet cutting quartz, chlorite and hematite (transmitted light). **f** Albite phenocryst replaced by orthoclase in altered dike (transmitted, cross-polarized light). *Ab* Albite; *Chl* chlorite; *Cpy* chalcopyrite; *Do* dolomite; *Hem* hematite; *Mt* magnetite; *Or* orthoclase; *Py* pyrite; *Qtz* quartz

of the Pardiac, Turcotte, and MdA showings (Fig. 10c). Hematite has low TiO_2 (0.02–0.41 wt%) and MgO (0.01–0.04 wt%) contents (Table 4). Ferroan dolomite, locally associated with late hematite, occurs as veins and veinlets crosscutting early-mineralized rocks (Table 5; Fig. 10e). Dolomite also fills open spaces interstitial to hematite, chlorite, and quartz.

Feldspar forms a major groundmass constituent as well as phenocrysts in mafic and felsic dikes. Groundmass feldspars (Table 6) are replaced by $albite_{93.6–98.9}$ or $orthoclase_{97.16–99.64}$ (Table 6). Orthoclase replaces albite in phenocrysts (Fig. 10f). Chlorite replaces feldspar phenocrysts in mafic and felsic dikes.

Chlorite geothermometry

Chlorite in mafic and felsic dikes, ore veins, fresh vesicular basalt, and in a potassic altered tuff have Fe/(Fe + Mg) ratios ranging between 0.35 and 0.80, and fall within the pycnochlorite and brunsvigite fields with minor ripidolite and diabantite chlorite (Fig. 11a; Table 7). Chlorite from mafic dikes have the largest range of Fe/(Fe + Mg) ratios (0.35−0.80), whereas felsic dikes have a larger range of Si_{IV} occupancy (2.7−3.4; Fig. 11a). Vein chlorite has a small range of Fe/(Fe + Mg) of 0.40–0.70 and Si_{IV} occupancy ranges from 2.8–3.1 (Fig. 11a). In contrast, chlorite from a potassic altered tuff has a lower Fe/(Fe + Mg) ratio (0.34), and a higher Si_{IV} occupancy around 3. The silicon and aluminum occupancy in the tetrahedral sites of all chlorite samples ranges from $Si_{2.73}$ $Al_{1.27}$ to $Si_{3.18}$ $Al_{0.82}$.

The Al–Si substitution in tetrahedral sites in chlorite increases with temperature (Cathelineau and Nieva 1985; De Caritat et al. 1993). Cathelineau (1988) showed that this substitution yields a geothermometer that is valid for temperatures ranging from 130 to 300°C. Chlorite from vesicular basalt yield temperatures of 229−248°C (average=238±8°C; n=4; Fig. 11b). Chlorite from a potassic altered tuff characterized by abundant orthoclase pheno-

Table 4 Representative microprobe composition of hematite from the Mont-de-l'Aigle deposit, Gaspé Peninsula, Quebec

Sample no.	220515	217822	217894
Analysis no.	Hem 1	Hem 1	Hem 2
SiO_2 (wt%)	0.33	0.31	0.02
TiO_2	0.02	0.02	0.05
Al_2O_3	0.73	0.05	1.03
Cr_2O_3	ND	0.06	ND
MgO	0.03	ND	ND
CaO	0.25	0.13	ND
MnO	ND	ND	ND
Fe_2O_3[a]	99.35	99.89	98.70
Total	100.71	100.46	99.80
Structural formula calculated on the basis of six oxygens			
Si	0.02	0.02	0.00
Al	0.05	0.00	0.00
Ti	0.00	0.00	0.06
Cr	0.00	0.00	0.00
Mg	0.00	0.00	0.00
Ca	0.01	0.01	0.00
Mn	0.00	0.00	0.00
Fe	3.92	3.97	3.93

ND Not detected
[a]Total Fe as Fe_2O_3

crysts yield temperatures of 204–225°C with an average of 215±11°C (n=3; Fig. 11b; Table 7). Chlorite from mafic intrusions yield temperatures of 252–347°C (average=302±22°C; n=31), whereas chlorite from felsic intrusions yield temperatures of 231–332°C (average=300±32°C; n=8; Fig. 11b; Table 7). Chlorite from veins yield temperatures of 242–319°C (average=289±20°C; n=17; Fig. 11b).

Table 5 Representative microprobe composition of dolomite from the Mont-de-l'Aigle deposit, Gaspé Peninsula, Quebec

Sample no.	MdA-04-02	217822	D26	217831
Analysis no.	Cb 2	Cb 5	Cb 1	Cb 2
$Mg(CO_3)$ (wt%)	35.23	34.83	34.47	39.31
$Ca(CO_3)$	53.50	52.63	53.17	53.34
$Mn(CO_3)$	2.11	1.04	1.23	1.31
$Fe(CO_3)$	8.90	12.10	11.24	5.83
Total	99.73	100.60	100.10	99.80
Structural formula calculated on the basis of six oxygens				
Mg	0.80	0.79	0.78	0.88
Ca	1.02	1.00	1.01	1.01
Mn	0.04	0.02	0.02	0.02
Fe	0.14	0.20	0.19	0.10

Table 6 Representative microprobe composition of feldspar from mafic and felsic intrusions from the Mont-de-l'Aigle deposit, Gaspé Peninsula, Quebec

	Orthoclase (unaltered)	Feldspar phenocryst		Groundmass feldspar	
		Or	Ab	Or	Ab
Analysis no.	F 4	Fd 4	Fel 9	Fel 7	F 5
Sample no.	218833	217432	217898	MdA-04-04	218831
SiO_2 (wt%)	64.83	63.89	68.99	61.84	68.00
Al_2O_3	19.53	18.95	20.36	21.16	20.43
MgO	0.01	0.08	0.00	0.07	0.02
CaO	0.61	0.01	0.28	0.04	0.11
FeO[a]	0.12	0.20	0.11	0.31	0.33
Na_2O	2.57	0.35	11.20	0.33	11.73
K_2O	12.00	15.66	0.07	14.95	0.09
Total	99.65	99.13	101.02	98.70	100.71
Structural formula calculated on the basis of eight oxygens					
Si	2.96	2.97	2.98	2.89	2.96
Al	1.05	1.04	1.04	1.16	1.05
Mg	0.00	0.01	0.00	0.01	0.00
Ca	0.03	0.00	0.01	0.00	0.01
Fe	0.00	0.01	0.00	0.001	0.01
Na	0.23	0.03	0.94	0.03	0.10
K	0.70	0.93	0.00	0.89	0.01
An	4.03	0.08	2.39	0.19	0.91
Ab	16.93	2.17	97.02	2.33	98.33
Or	79.04	97.75	0.60	97.48	0.76

ND Not detected
[a]Total Fe as FeO

Alteration

Alteration of mafic and felsic dikes forms in three stages: I) early, weak sodic alteration proximal to mineralization, mainly in mafic rocks; II) peripheral potassic alteration (± Ca); and III) late, pervasive chlorite ± silica alteration distal from mineralization. In sedimentary rocks, alteration is less obvious in the field and is divided into three facies: I) proximal alkali leaching, decalcification and silicification; II) weak potassic alteration with minor enrichment in sodium, and III) distal pervasive chlorite ± silica alteration associated with iron enrichment. Element mobility during alteration was quantified by plotting immobile elements (Al, Zr, Ti, Y, Nb, and HREE) in isocon plots (Grant 1986).

Stage I sodic alteration (up to 6 wt% Na_2O) is recognized in type 3 and some type 1 dikes. Albite phenocrysts coexist with euhedral fluoroapatite, disseminated in the groundmass. The feldspar-rich groundmass is replaced by dolomite or is cut by late dolomite veinlets (Fig. 10e). Stage I alteration in type 3 dikes shows that the heavy REE were immobile during alteration and plot close to a line of constant mass with a slope of 1.02 (Fig. 12a). In stage I alteration mass gains are apparent in CaO, Na_2O,

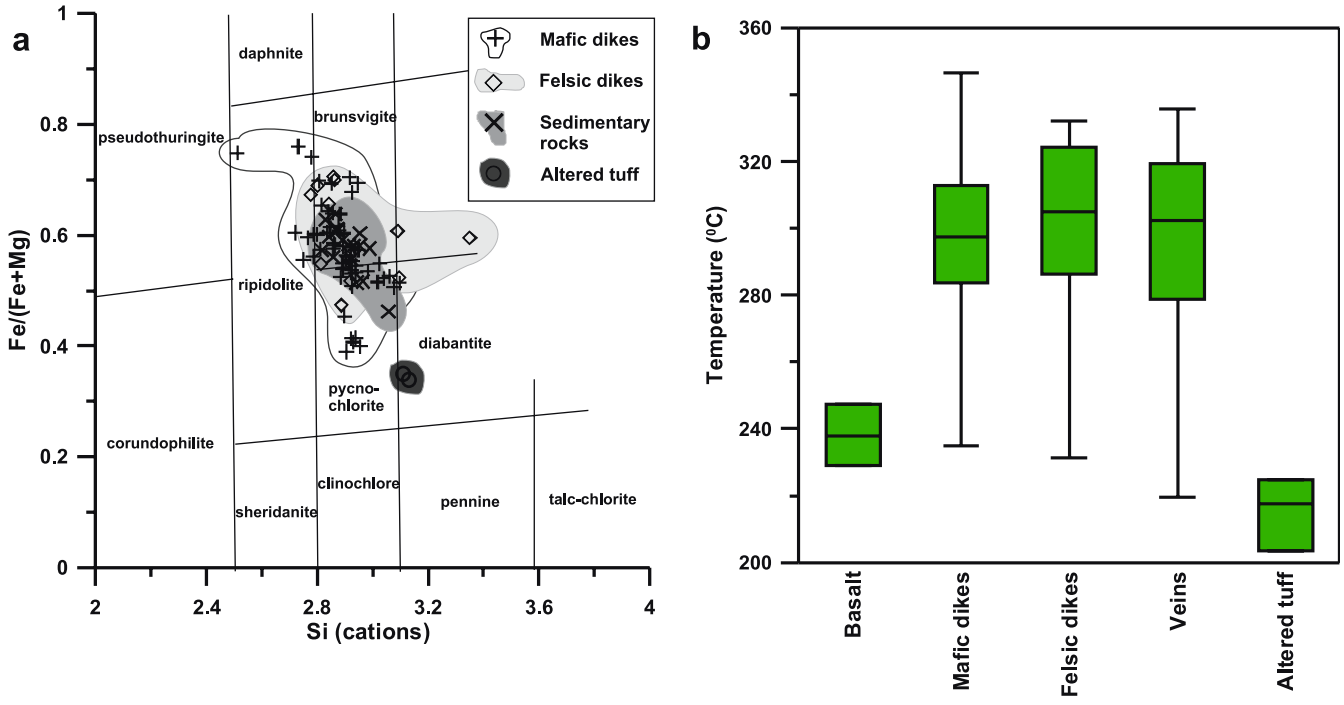

Fig. 11 Chlorite chemistry from mafic and felsic dikes, fresh vesicular basalt, veins, and a potassic altered tuff, from the Mont-de-l'Aigle deposit. **a** Fe/(Fe + Mg) vs Si cations for chlorite (Hey 1954). **b** Calculated temperature plot from the Al^{IV} chlorite thermometer (Cathelineau 1988)

MnO, and Zn, whereas mass losses in K_2O, Ba, Sr, MgO, Fe_2O_3, TiO_2, and Rb occur.

Stage II potassic alteration (up to 8 wt% K_2O) overprints stage I in mafic and felsic dikes and is characterized by orthoclase, quartz, dolomite, fluoroapatite, and minor chlorite and epidote. Euhedral orthoclase replaces albite phenocrysts (Fig. 10f). The groundmass of potassic altered dikes is composed of fine-grained quartz and dolomite. Potassic alteration comprises orthoclase ± quartz veinlets cutting stage I alteration. HREE, Nb, and Zr from stage II alteration in type 3 dikes plot close to or on a line of constant mass with a slope of 1.11 (Fig. 12b). This potassic zone displays mass gains in Rb, Ba, K_2O, and Sr, whereas Na_2O, MgO, Fe_2O_3, and MnO are depleted. Stage II alteration is accompanied by a slight enrichment in LREE. Stage II alteration in some types 1 and 2 dikes is accompanied by a calcic alteration characterized by epidote and dolomite.

Stage III chlorite (± quartz) alteration occurs as veinlets, replacement of orthoclase phenocrysts, and as pervasive replacement of groundmass cutting stage II alteration. Immobile elements Ta, Nb, Ti, and Al from stage III alteration in type 4 dikes plot close to or on a line of constant mass with a slope of 0.93 (Fig. 12c). Co, Fe_2O_3, MgO, and LOI are enriched in stage III chlorite zone whereas Na_2O, CaO, REE, and Ba are depleted.

For sedimentary rocks, the composition of fresh limestone from the Forillon Formation was used as the least-altered sample (Pilote and Lachance 2003). Facies I alkali leaching, decalcification, and silicification is characterized by $K_2O + Na_2O \leq 1.85$ wt%, CaO ≤0.72 wt%, and SiO_2 up to 67 wt%. In facies I of the Forillon Formation, REEs were immobile, plotting along a line with a slope of 0.93 (Fig. 12d). In this zone, MnO, Fe_2O_3, Zn, Co, and MgO are enriched, whereas CaO, Sr, Rb, K_2O, Na_2O, Ba, and LOI are depleted. The large decrease in LOI is most likely due to intense decalcification. Zr, Nb, and Ti, however, plot off the isocon line, possibly due to a compositional heterogeneity in the heavy mineral fraction of the sedimentary rocks (Fig. 12d).

Facies II potassic alteration (up to 5.84 wt% K_2O) also caused a minor enrichment in sodium (up to 2 wt% Na_2O). REE in facies II altered limestone from the Forillon Formation plot along a line with a slope of 2.11 (Fig. 12e). The altered samples are enriched in Ba, Co, MnO, Fe_2O_3, Ni, K_2O, and Zn and depleted in CaO, LOI, and Sr. The enrichment in potassium is marked by minor sericite in the alteration assemblage and the large LOI depletion indicates intense decalcification.

Facies III chlorite ± silica alteration is peripheral to facies I and II alteration. The chlorite ± silica alteration is associated with a Fe-enrichment (FeO_T up to 24 wt%). REE in facies III alteration of Forillon Formation were immobile, plotting along the isocon line with a slope of 1.52 (Fig. 12f). In this zone, Co, Fe_2O_3, MnO, Zr, Cu, Ni, TiO_2, Ba, and Zn are enriched whereas CaO, LOI, Rb, and Na_2O are depleted. The enrichment in Co, Fe, and Mn is related to pervasive chloritization. No temporal relationship is observed between facies I, II, and III alteration in sedimentary rocks.

A summary of the distribution of alteration types in intrusion and sedimentary rocks in relationship with Cu–Fe (± Au) mineralization is presented in Fig. 13. The type of alteration changes with the host rock type. Mafic intrusive

Table 7 Representative microprobe composition of chlorite and calculated temperature from Cathelineau (1988) from the Mont-de-l'Aigle deposit, Gaspé Peninsula, Quebec

	Basalt		Mafic intrusions		Felsic intrusions	Veins	Altered tuff	
Analysis no.	Chl 1	Chl 2	Chl 3	Chl 5	Chl 2	Chl 1	Chl 7	Chl 1
Sample no.	MdA-04-02	218833	217894	217911	217432	220515	D26	MdA-04-04
SiO_2	28.67	27.25	24.93	26.39	29.43	26.45	27.03	31.64
TiO_2	ND	ND	ND	ND	ND	ND	ND	ND
Al_2O_3	15.02	17.13	17.51	19.90	20.81	18.64	16.74	17.42
Cr_2O_3	ND	ND	ND	0.05	ND	0.05	ND	0.06
MgO	14.86	14.19	7.65	8.16	9.59	11.87	12.53	20.49
CaO	0.15	0.11	0.02	0.03	0.06	0.10	0.25	0.43
MnO	0.34	0.45	0.69	0.57	1.26	0.45	0.57	0.34
FeO[a]	29.43	28.67	39.06	33.80	26.50	31.37	30.96	18.89
NiO	ND	ND	ND	ND	ND	ND	ND	ND
Na_2O	ND	ND	ND	0.05	0.08	ND	0.05	ND
H_2O	11.24	11.18	10.76	11.06	11.42	11.17	11.06	12.11
Total	99.76	99.05	100.69	100.03	99.17	100.10	99.25	101.51
Structural formula calculated on the basis of 14 oxygens								
Si^{IV}	3.06	2.92	2.78	2.86	3.09	2.84	2.93	3.13
Al^{IV}	0.94	1.08	1.22	1.14	0.91	1.16	1.07	0.87
Ti	ND	ND	ND	ND	ND	ND	ND	ND
Cr	0.00	0.00	0.00	0.00	0.00	0.00	0.00	0.01
Mg	2.36	2.27	1.27	1.32	1.50	1.90	2.03	3.02
Ca	0.02	0.01	ND	ND	0.01	0.01	0.03	0.05
Mn	0.03	0.04	0.07	0.05	0.11	0.04	0.05	0.03
Fe	2.63	2.57	3.64	3.07	2.33	2.82	2.81	1.56
Ni	ND	ND	ND	ND	ND	ND	ND	ND
Na	ND	0.01	0.01	0.01	0.02	ND	0.01	0.01
X_{Fe}	0.53	0.53	0.74	0.70	0.61	0.60	0.58	0.34
T (°C)	241	285	331	304	231	311	282	217

ND Not detected
[a]Total Fe determined as FeO

rocks have stage I alteration surrounded by stage II alteration, whereas felsic intrusive rocks display a large zone of stage II alteration. Sedimentary rocks show a proximal facies I surrounded by facies II alteration. No feldspar phenocryst is observed in facies II alteration and the potassium enrichment is lower than in stage II alteration in mafic and felsic dikes. Both altered igneous and sedimentary rocks display pervasive distal chlorite alteration, associated with Fe enrichment in sedimentary rocks.

Stable isotope geochemistry

The S isotope composition range from −0.8 to 4.8‰ for pyrite (n=9, average=1.8±1.6‰) and from −1.5 to 2.8‰ for chalcopyrite (n=7, average=0.5±1.3‰; Fig. 14a; Table 8). Overall, the sulfides have an isotopic signature around 0‰ consistent with a magmatic source for the sulfur. Pyrite and chalcopyrite pairs are not in textural equilibrium and yield calculated temperatures of 75 to 416°C using Kajiwara and Krouse (1971) that indicate isotope disequilibrium as well.

$\delta^{18}O$ values range from 6.5 to 9.5‰ for quartz (n=19, average=7.7±0.9‰) and from −10.4 to −5.9‰ for hematite (n=3, average=−8.1±2.2‰; Fig. 14b; Table 8). Quartz–hematite pairs (Table 8) yield isotope equilibrium at temperatures between 251 and 328°C, using Zheng (1991).

Discussion

Intrusions

The REE patterns of mafic dikes reflect evolution from primitive, less differentiated magma of type 1 dikes to more differentiated magma of type 3 dikes (Figs. 3 and 5). Type 1 dikes are similar to alkaline basalts of the York River Formation (Fig. 4a; Doyon and Valiquette 1991). Types 1 and 2 dikes do not have negative Eu anomalies (Fig. 3a,b), suggesting no significant plagioclase fractionation. Alter-

natively, the absence of a negative Eu anomaly may indicate a magma with a relatively high oxidation state (Eu^{+3}) in which the partition coefficient for Eu between plagioclase and melt is low, such that Eu behaves similarly to other rare-earth elements (Marschick et al. 2003). Type 3 dikes have high REE contents and negative Eu anomaly suggesting derivation via fractional crystallisation of type 1 magma (Figs. 3c and 5b). The fractionated REE patterns of type 4 dikes are similar to that of rhyolite from the York River Formation (Figs. 3d and 4a; Doyon and Valiquette 1991). Type 4 dikes have negative Eu anomalies indicative of fractionation via plagioclase crystallization.

Intrusions at the Mont-de-l'Aigle deposit are coeval with felsic volcanism of the York River Formation. Whalen et al. (1994) suggested that melting of the crust during the Siluro–Devonian was likely associated with lithospheric

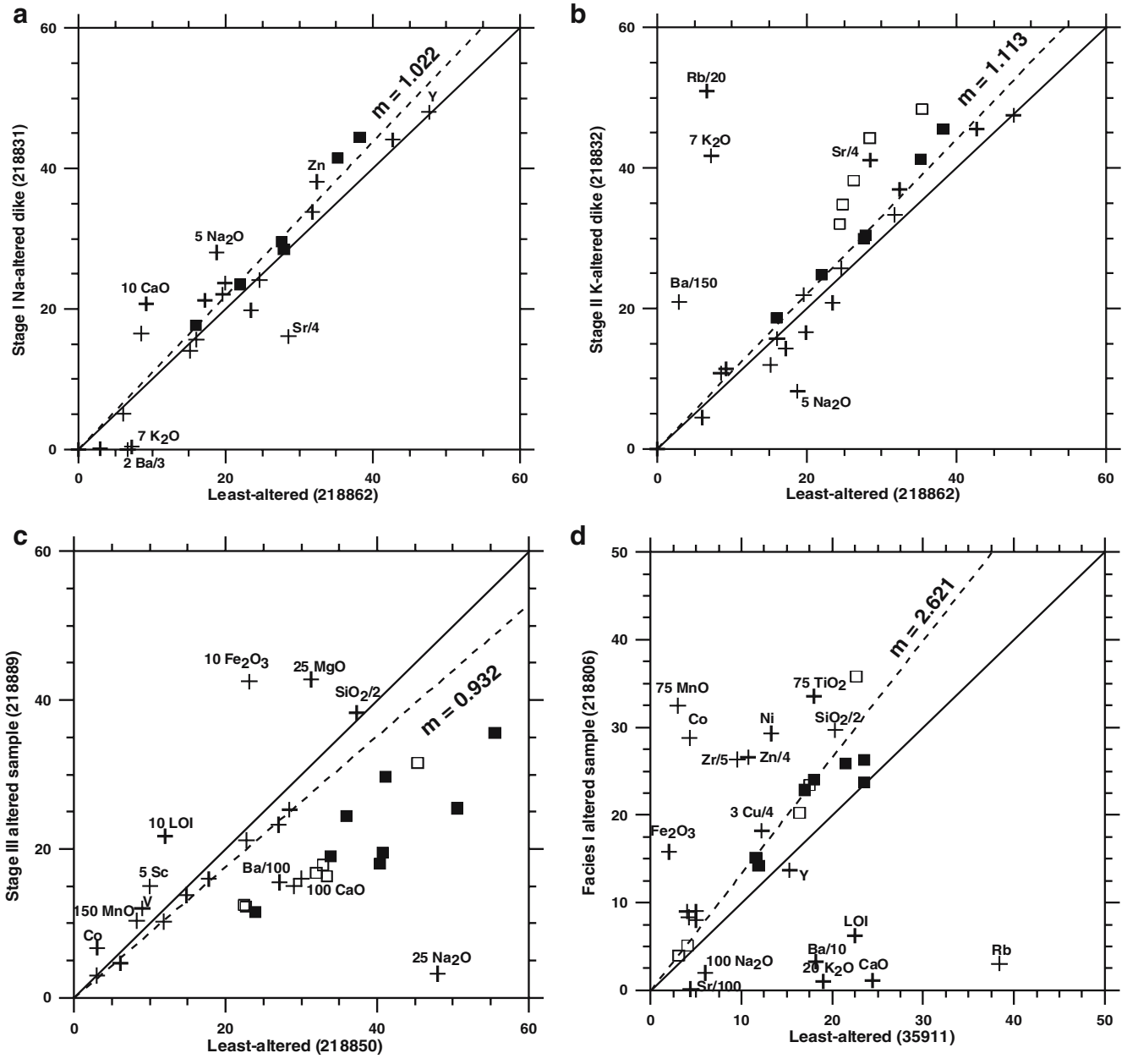

Fig. 12 Isocon diagrams for intrusions and sedimentary rocks calculated according to Grant (1986). **a** Comparison of representative stage I alteration type 3 dike (218831), with least-altered type 3 dike (218862). **b** Comparison of representative stage II alteration type 3 dike (218832) with least-altered type 3 dike (218862). **c** Comparison of representative stage III alteration type 4 dike (218889) with least-altered type 4 dike (218850). **d** Comparison of representative facies I alteration (218806), with representative least-altered Forillon Formation (35911). **e** Comparison of representative facies II alteration (218818) with representative least-altered Forillon Formation (35911). **f** Comparison of representative facies III alteration (218805) with representative least-altered Forillon Formation (35911). The isocon (*dashed line*) with slope (m) is drawn through immobile elements. Elements that display important mass gains or losses are labeled. *Filled squares* represent heavy rare earth elements, whereas *open squares* are light rare earth elements. Data from Table 1 and Appendix. Least-altered Forillon Formation sample 35911 is from Pilote and Lachance 2003

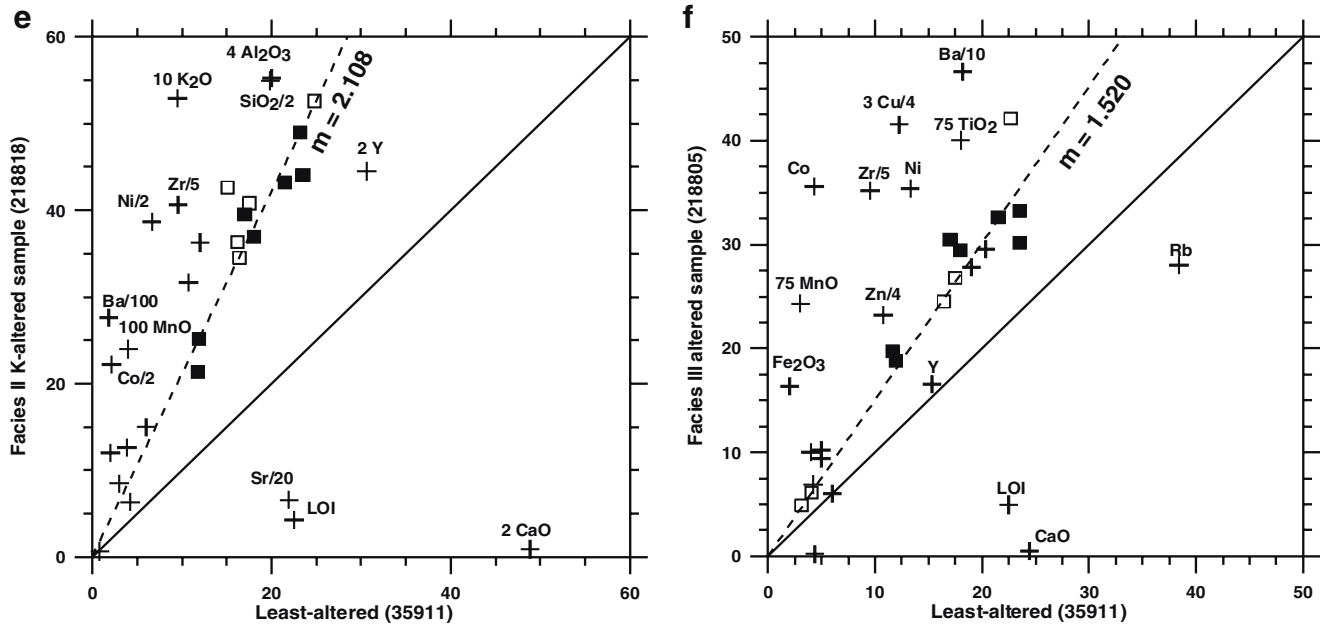

Fig. 12 (continued)

delamination or crust–mantle detachment. Transitional granites were derived from this lithospheric delamination as a result of extension and collapse of the crust, thinning of the lithosphere and rise of hot asthenosphere after compressive deformation had ceased (Winter 2001). The mafic magmas are interpreted to have reached surface via

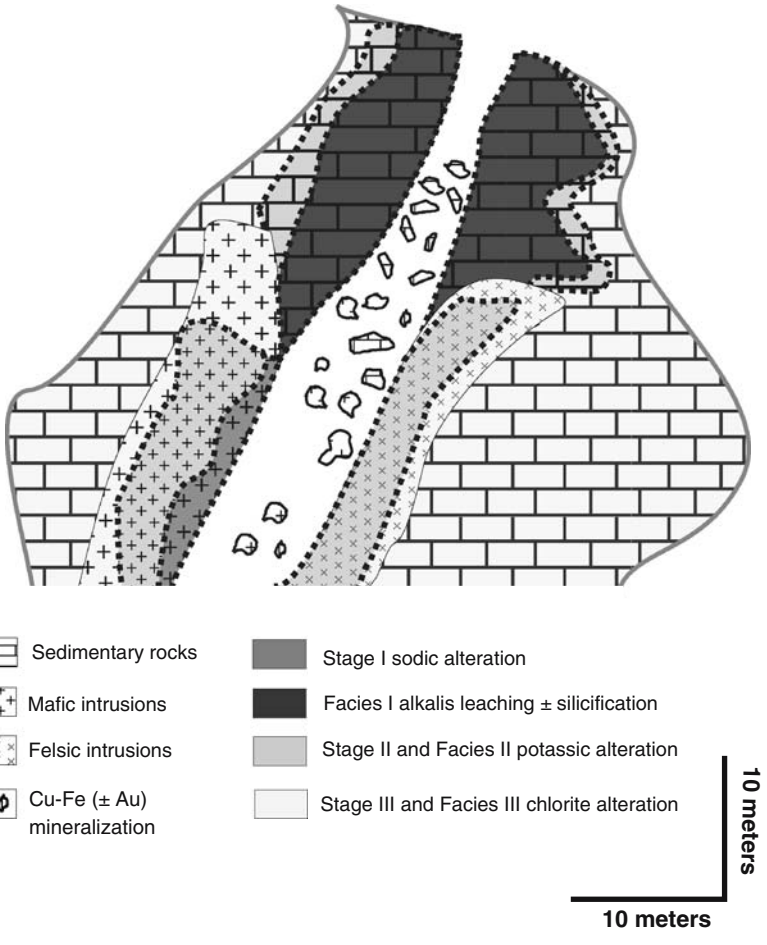

Fig. 13 Schematic representation of the spatial relationship between alteration stages and facies in intrusions and sedimentary rocks and Cu–Fe (± Au) mineralization

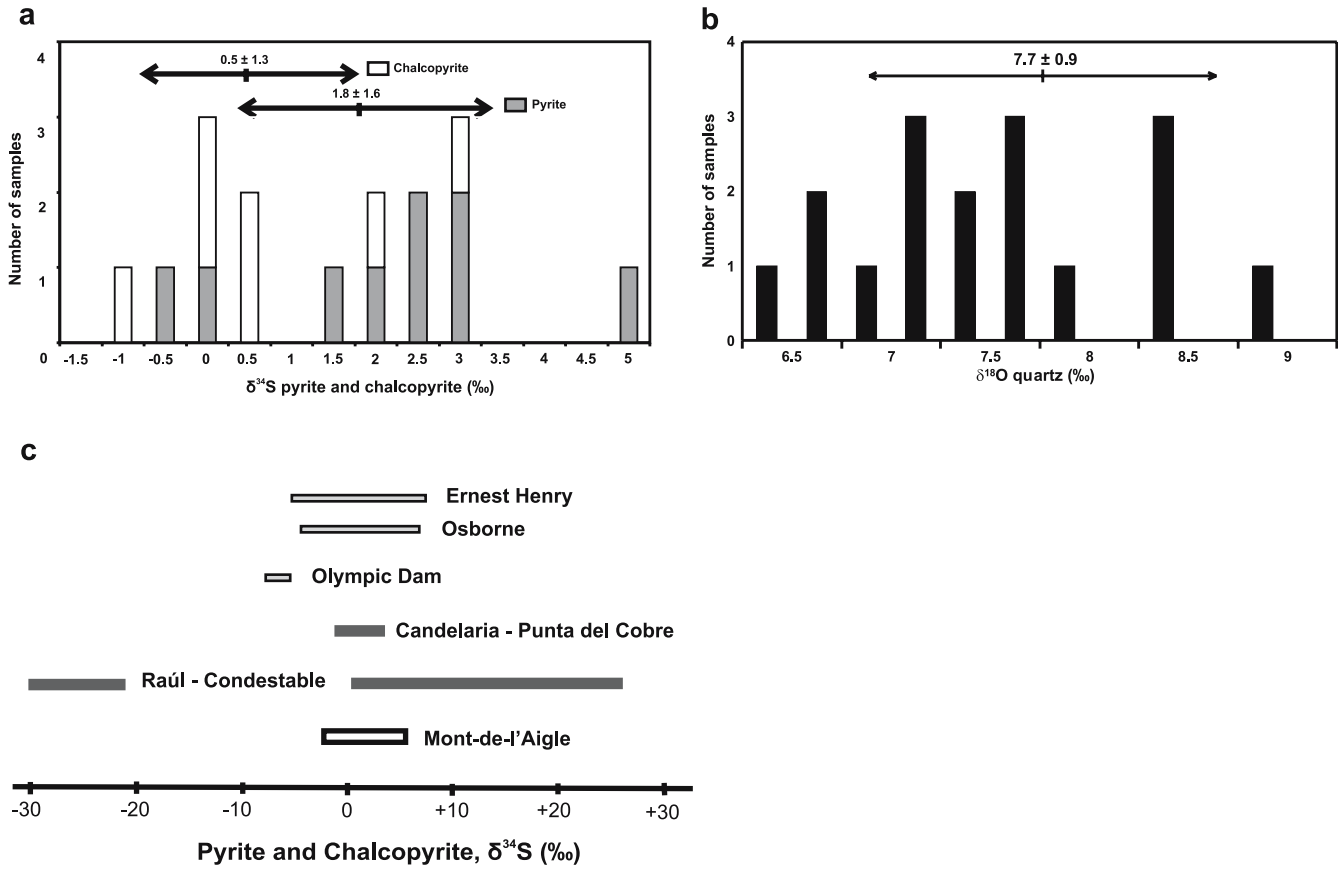

Fig. 14 Distribution of sulfur and oxygen stable isotopes in the Mont-de-l'Aigle deposit (Table 8). **a** $\delta^{34}S$ values for pyrite and chalcopyrite. **b** $\delta^{18}O$ values for quartz. **c** Range in $\delta^{34}S$ for selected IOCG deposits: Osborne, Ernest Henry (Williams and Pollard 2001), Olympic Dam (Mark et al. 2002), Candelaria–Punta del Cobre and Raúl Condestable (Sillitoe 2003)

normal faults in an extensional setting. This is consistent with the close spatial relationship between intrusions and faults (Figs. 2 and 8). Heat from upwelling mantle generated partial melt in crustal rocks producing felsic magmas and accounts for bimodal magmatism in extensional settings (Winter 2001). The Lemieux Intrusive Suite was likely derived from intracontinental orogenic collapse decompressional melting after regional compression during the Acadian Orogeny. The Tb–Ta data (Fig. 5b) supports the interpretation that mafic intrusions were derived from similar parent magma via fractional crystallization whereas, type 4 dikes were derived from partial melting of continental crust. Pearce et al. (1984) suggested that depleted rhyolites (Y≤25 ppm; Fig. 5a) overlapping the field of volcanic arc granite and collisional-granite in the Nb vs Y diagram, such as type 4 dikes (Fig. 5c), were likely derived from partial melting of the continental crust. Type 4 felsic dikes are chemically similar to the dacitic porphyry of the Sullipek–Est and Copper Mountain (Mines Gaspé) deposits (Wares 1983).

The Siluro–Devonian dikes at the Mont-de-l'Aigle deposit are older than Cu–Fe (± Au) mineralization and alteration, but they could be precursors of the hydrothermal system. As with many IOCG deposits worldwide (Ray and Webster 2000; Sillitoe 2003; Williams et al. 2005), the Mont-de-l'Aigle deposit does not appear to be spatially related to a specific intrusion. Intrusions at the Mont-de-l'Aigle deposit (398.3±0.8 Ma; Pilote and Lachance 2003) are older than those at Mines Gaspé deposits (384.9± 2.5 Ma) and the McGerrigle plutonic complex (391.9± 3.4 Ma) (Whalen et al. 1991; Stephenson et al. 1998), perhaps indicating that they were a precursor of widespread regional felsic plutonism.

Comparison of the Mont-de-l'Aigle deposit with IOCG, porphyry, and skarns deposits

The Mont-de-l'Aigle deposit displays several characteristics similar to those of IOCG deposits, whereas other characteristics are atypical of IOCG deposits. To classify the Mont-de-l'Aigle deposit, its significant attributes are compared to those of Candelaria–Punta del Cobre, Olympic Dam and Wernecke Moutains IOCG, Mines Gaspé Cu–Mo porphyry and Sullipek Cu-skarn deposits (Table 9).

Paleozoic IOCG deposit are uncommon but some examples include stratiform and diatreme-shaped iron deposits in the Bafq-Seghand district in central Iran (Taghizadeh 1977; Förster and Knittel 1979; Förster

Table 8 Stable isotope data from the Mont-de-l'Aigle deposit, Gaspé Peninsula, Quebec

Showing	Sample no.	Description	$\delta^{18}O$ (‰, V-SMOW)		$\delta^{34}S$ (‰, V-CDT)	
			Quartz	Hematite	Pyrite	Chalcopyrite
Frenette	162297	Qtz-hem-mt vein	8.9			
	220579	Qtz vein	7.7			
Brèche-Rio	189603	Qtz vein	7.8			
	217887	Cement of breccia	6.6			
	217915	Cement of breccia	8.3			
	217919	Cement of breccia	7.7			
	217923	Cement of breccia	9.4			
	217927	Cement of breccia	7.4			
	217933	Hem-qtz vein	7.7	−10.4		
East of Pardiac	218005	Cement of breccia	6.7			−1.5
	218006	Cement of breccia			2.2	
Porphyre	217813	Massive py-cpy vein			1.6	
	217937	Brecciated vein				2.8
Pardiac	217844	Cement of breccia	7.1			
	217903	Cement of breccia				1.9
	217938	Hematite vein	7.0			
	217939	Hem-py vein			2.7	
	220502	Hem-py vein cutting black mudstone			−0.8	
	220504	Hem-py vein cutting black mudstone	7.5			
	220505	Hem-py-mt vein cutting black mudstone			4.8	
	220507	Hem-py vein cutting black mudstone	7.1			
	220508	Hem-py-cpy vein cutting black mudstone				−0.3
	220513	Hem-py vein cutting black mudstone		−5.9	−0.2	
	220516	Hem-py vein cutting black mudstone				0.0
	220520	Hem-py vein cutting black mudstone	6.5			
	220523	Hem-py vein cutting black mudstone		−8.1		
	220578	Stockwork			2.5	
Hupé	189617	Cement of breccia	9.5			
	189618	Cement of breccia	8.5			
	217876	Stockwork	8.5			
Duchesne	189634	Stockwork	7.1			
	189646	Stockwork			2.6	
	218008	Disseminated in black limy mudstone			1.2	
	218010	Disseminated in black limy mudstone				0.3
	D26	Hem-cpy-mt vein				0.4

Cpy Chalcopyrite, *Hem* hematite, *Mt* magnetite, *Py* pyrite, *Qtz* quartz

1990; Hitzman et al. 1992), stratiform deposits in the Avnik district of southeasthern Turkey (Helvaci 1984; Hitzman et al. 1992) and massive hematite veins in the Rotliegends volcanic rocks, Germany (Schmidt Mumm and Wolfgramm 2004). Carbonate host rocks are unusual for IOCG type deposits, although IOCG deposits hosted by carbonate-bearing sequences are recognized at Candelaria–Punta del Cobre, Chile, and Cloncurry, Australia (Table 9; Mark et al. 2002; Marschick and Fontboté 2001; Sillitoe 2003; Mark et al. 2004; Oliver et al. 2004). Several Lower Cretaceous IOCG deposits in the Coastal Cordillera of Chile are hosted by clastic sedimentary (sandstone, conglomerate) and volcanic rocks such as the Teresa Colmo deposit (Hopper and Correa 2000). The Wernecke Mountains deposit (Yukon, Canada) includes breccia bodies cutting Middle Proterozoic mudstone, siltstone, and dolostone (Table 9; Lane 1990; Hitzman et al. 1992; Hunt et al. 2005). Some IOCG deposits are interpreted to form where a contact metamorphic aureole is affected by circulating hydrothermal fluids after peak metamorphism (Pollard 2002). Hornfels occurs at depth at the Mont-de-l'Aigle deposit (Fig. 8; Bellehumeur and Valiquette 1993). At Mines Gaspé, a Devonian porphyry associated with Cu-skarn deposits is in contact with calc-silicate hornfels in

Table 9 Comparison of the Mont-de-l'Aigle deposit and other magmatic-hydrothermal deposits

	Mont-de-l'Aigle deposit, Canada	Candelaria–Punta del Cobre, Chile	Olympic Dam, Australia	Wernecke Mountains, Canada	Mines Gaspé, Canada	Sullipek, Canada
Host rocks	Limestones, siltstones, mafic and felsic intrusions	Volcanic and volcaniclastic rocks, limestone	Intrusions, volcaniclastic, sedimentary rocks	Clastic sedimentary rocks	Limestones, felsic intrusions	Limestones, felsic intrusions
Age mineralization	Siluro–Devonian (<398 Ma)	Cretaceous (115 Ma)	Proterozoic	Proterozoic	Paleozoic (384.9±2.5 Ma)	Paleozoic
Metamorphism	Sub-greenschist	Greenschist to amphibolite	Sub-greenschist	Greenschist to amphibolite	Contact metamorphism, greenschists	Contact metamorphism, greenschists
Tectonic setting	Intracontinental orogenic collapse	Back-arc basin	Anorogenic	Intracratonic basin	Intracontinental orogenic collapse	Intracontinental orogenic collapse
Deposit style	Breccias, stockworks, veins	Veins, breccias, replacement and stringer bodies	Breccias	Breccias	Skarns, veins, stockworks	Skarns, hornfels, veins
Sulfur isotopes	−1.5 to 4.8‰	−0.7 to 3.1‰	−6 to −9‰		6 to 12‰	
Fluids inclusions	T=280–347°C, Salinity = 0–26 wt% NaCl equivalent	T=220–310°C, Salinity = 12–24 wt% NaCl equivalent	T=100–300°C, Salinity = 7–42 wt% NaCl equivalent		T=150–350°C Salinity = 15–47 wt% NaCl equivalent	
Ore mineralogy	Hematite, chalcopyrite, pyrite, magnetite	Magnetite, hematite, chalcopyrite, pyrite	Hematite, pitchblende, pyrite, chalcopyrite, chalcocite, bornite	Magnetite, hematite, pyrite, chalcopyrite	Pyrrhotite, chalcopyrite, molybdenite, pyrite	Pyrite, chalcopyrite, molybdenite, bornite
Alteration	Sodic, potassic, decalcification, silicification, chloritization	Calcic, potassic, sodic, carbonatization	Hematite and sericite alteration, silicification, potassic	Potassic, sericitic, sodic, bleaching	Skarns, hornfels, argillic, sericitic, potassic, bleaching	Skarns, hornfels, sodic, potassic, sericitic

Candelaria Marschik and Fontboté 2001; Sillitoe 2003; Marschik et al. 2003, *Olympic Dam* Hitzman et al. 1992; Haynes et al. 1995; Hitzman 2000; Pollard 2002, *Wernecke Mountains* Laznicka and Edwards 1979; Hitzman et al. 1992; Thorkelson et al. 2001, *Mines Gaspé* Shelton and Rye 1982; Allcock 1982; Shelton 1983, *Sullipek* Wares 1986

rocks of the Shiphead Formation (Table 9; Allcock 1982; Shelton 1983).

Pollard (2002) suggested that intrusions associated with IOCG deposits are typically granite that formed by partial melting of older middle to lower crusted rocks with a variable mantle input (Table 9; Creaser 1996; Pollard et al. 1998). In several IOCG deposits, such as Mantoverde and Candelaria–Punta del Cobre, mineralization is distal to plutonic complexes, but yields ages similar to those of the plutons (Sillitoe 2003; Williams et al. 2005). Sillitoe (2003) suggested a close genetic relationship between IOCG deposits in northern Chile and plutons with dioritic composition.

The tectonic setting for the Mont-de-l'Aigle deposit intrusive rocks is most likely an intracontinental orogenic collapse, one of the end-member tectonic environments typical for IOCG deposits (Table 9; Hitzman 2000). The Olympic Dam deposit formed in an anorogenic setting characterized by voluminous felsic plutonic and volcanic rocks with lesser mafic igneous rocks (Table 9; Hitzman 2000). Mines Gaspé and Sullipek deposits likely formed in an extensional setting that is atypical for porphyry and skarn deposits, that are typically found in oceanic or continental convergent margins (Guilbert and Park 1986; Meinert 1993; Doyon and Berger 1997).

Veins and breccia matrix of the Mont-de-l'Aigle deposit have $\delta^{18}O$ values ranging from 6.5 to 9.5‰ (Table 8; Fig. 14b). The $\delta^{18}O$ values for the fluid from which quartz precipitated ranged from −0.4 to 2.6‰ at 300°C using Clayton et al. (1972), indicating that meteoric or seawater had reacted with the country rocks. Salinity of fluid inclusions in hematite-chalcopyrite from the northern part of Dome Lemieux (0–26 wt% NaCl equivalent; Stevens 1986) overlaps the lower range of salinities reported for Olympic Dam (7–42 wt% NaCl equivalent; Haynes et al. 1995). Salinity from the Mont-de-l'Aigle deposit is comparable to that of Candelaria–Punta del Cobre district (12–24 wt% NaCl equivalent; Marschick and Fontboté 1996). Lower salinity in mineralization of the Mont-de-l'Aigle deposit could explain the limited albitization (Na-addition) relative to the regionally extensive albitization in IOCG deposits that is associated with high salinity fluids (Pollard 2001, 2002; Oliver et al. 2004).

The Mont-de-l'Aigle deposit $\delta^{34}S$ values range from −1.5 to 4.8‰, overlapping those of Australian and Andean IOCG deposits that are near 0‰ (Fig. 14c), and that indicate a magmatic source of sulfur. The composition of this magmatic sulfur may reflect a component derived via leaching of the underlying volcanic rocks or a direct contribution from magmatic fluids. The hydrothermal fluids that formed the Mont-de-l'Aigle deposit could be the result of mixing of a saline magmatic fluid with meteoric water, a model proposed for Olympic Dam and Candelaria–Punta del Cobre (Haynes et al. 1995; Marschick and Fontboté 2001). Sulfide $\delta^{34}S$ values at Mines Gaspé are relatively uniform near −1‰ suggesting also an igneous source for the sulfur (Shelton and Rye 1982; Shelton 1983).

Fe-rich chlorite composition shows no variation with respect to the composition of host rocks (Fig. 11a), indicating that chlorite composition was controlled primarily by the fluid and therefore a high fluid/rock ratio. Temperatures estimated from Mont-de-l'Aigle deposit chlorite are higher in altered intrusions and veins (280–347°C) than in basalt and potassic tuff (204–248°C; Fig. 11b), possibly distinguishing hydrothermal chlorite from low-grade metamorphic chlorite. Chlorite formed during the late alteration stage (post-hematite) may not record the peak temperature of the hydrothermal system. The temperature range of hydrothermal chlorite is comparable to the range in oxygen isotope equilibrium temperatures of quartz–hematite (251–328°C). The chlorite temperatures are within the range of fluid inclusions homogenization temperatures (295–460°C; Stevens 1986) for development of hematite–pyrite–chalcopyrite veins of the northern part of Dome Lemieux. The temperature range is also comparable to that estimated from chlorite at Punta del Cobre, Chile (220–310°C; Table 9; Marschick and Fontboté 1996) and at Starra, Australia (319–366°C; Rotherham 1997b). It is at the higher end of the temperature range (100–300°C) proposed by Hitzman et al. (1992) for high-level, hematite-dominated IOCG deposits (Table 9).

IOCG deposits are characterized by a wide range of low-gold grades (Sillitoe 2003). The Teresa del Colmo deposit, Chile has resources of 70 Mt at 0.8% Cu with only trace of gold (Hopper and Correa 2000; Sillitoe 2003), whereas the Osborne deposit from the Cloncurry district has resources of 11.2 Mt at 3.51% Cu and 1.49 g/t Au (Mark et al. 2002; Williams et al. 2005). The range of gold grades from the Mont-de-l'Aigle deposit (up to 2.2 g/t Au) is comparable to the range of gold grades in Andean IOCG (Sillitoe 2003).

The most distinctive feature of the Mont-de-l'Aigle deposit is the abundance of hematite mineralization (Table 9). Pseudomorphic replacement of this early hematite by magnetite (mushketovite) could indicate an increase in temperature and/or a shift to more reduced conditions during mineralization (Marschick and Fontboté 2001). Mushketovite is a typical feature of the Candelaria–Punta del Cobre deposit and is probably widespread in IOCG deposits (Rotherham 1997a; de Haller 2000; Marschick and Fontboté 2001; Requia et al. 2003). In deposits formed at shallow-levels where surficial fluids infiltrated in the hydrothermal system, alteration is dominantly sericitic, and the main iron oxide is typically hematite, whereas magnetite is dominant in deeper-seated deposits (Pollard 2002).

Australian IOCG deposits are characterized by low SiO_2 content, and the absence of quartz veins, whereas Andean IOCG deposit gangue mineralogy consists predominantly

of quartz and anhydrite at Candelaria, and calcite and/or quartz at Punta del Cobre (Marschick and Fontboté 2001; Sillitoe 2003). The Wernecke breccias are characterized by late, disseminated or vein, dolomite associated with specular hematite (Thorkelson et al. 2001; Hunt et al. 2005). At the Frenette showing, late N–S and NW–SE barite veins cut the hematite matrix-rich breccias, a characteristic similar to the Olympic Dam deposit (Hitzman et al. 1992) and the Cloncurry district (Mark et al. 2004).

Hitzman (2000) noted that some porphyry copper deposits contain alteration suites similar to those of IOCG deposits. IOCG deposits are generally associated with sodic-potassic, potassic, or sericitic alteration depending on the degree of interaction of the mineralizing fluid and host rocks (Table 9; Hitzman 2000). Hitzman et al. (1992) indicated that alteration in IOCG deposits is zoned with respect to depth, whereas porphyry deposits are associated with envelopes of potassic, propylitic, phyllic, and/or argillic alteration that are commonly centered on the porphyry intrusions related to mineralization (Corbett and Leach 1998). Regionally developed sodic–calcic alteration, typical of IOCG deposits formed deep in the crust (Hitzman 2000), may also occur in porphyry deposits such in the Ann-Mason deposit, Nevada where Dilles and Einaudi (1992) suggested that the sodic–calcic alteration resulted from influx of heated saline formation waters and pointed out that several other porphyry districts and a number of systems are hosted by sodic and calcic alteration. Oliver et al. (2004) concluded that albitization in the Cloncurry district resulted from mixing of magmatic S-bearing fluids and brines, the latter probably initially of igneous derivation, but extensively modified by wall-rock interaction. Lower temperature IOCG deposits show minor or no regional Na–Ca alteration, whereas potassic alteration is associated with hematite-rich deposits formed at shallow depth such as in the Candelaria–Punta del Cobre (Sillitoe 2003) and Olympic Dam deposits (Table 9; Hitzman et al. 1992). An early pervasive albitization preceded potassic alteration at the Punta del Cobre district (Marschick and Fontboté 1996, 2001); whereas the Wernecke breccias contain igneous clasts with primary plagioclase replaced by albite, potassium feldspar, and scapolite (Table 9; Thorkelson et al. 2001; Hunt et al. 2005). The large chlorite alteration zone at the Mont-de-l'Aigle deposit is similar to that observed at Mantoverde, Peru (Vila et al. 1996). At Olympic Dam, the intense sericite–chlorite alteration has been linked to hydrogen ion production during sulfate reduction (Haynes et al. 1995). Lack of significant sericite alteration at the Mont-de-l'Aigle deposit perhaps indicates that acidity instead was neutralized reaction with carbonate host rocks as recorded by decalcification proximal to the mineralization.

Genetic evolution of Mont-de-l'Aigle mineralization

The Mont-de-l'Aigle deposit displays features similar to those at other deposits in the Gaspé Peninsula where mineralization is associated with syn- to late Acadian porphyritic intrusions in Paleozoic calcareous rocks. Felsic dikes from the Mont-de-l'Aigle deposit are geochemically similar to those associated with Mines Gaspé and the Sullipek deposit but they are older (398 Ma) than the felsic dikes from Mines Gaspé (385 Ma; Fig. 5a,b; Stephenson et al. 1998; Pilote and Lachance 2003). Epithermal quartz–sphalerite–galena–carbonate–amethyst veins at Mine Federal are interpreted to be coeval with felsic volcanism of the York River Formation (Stevens 1986). This epithermal mineralization is older than the IOCG mineralization because amethyst fragments occur in Mont-de-l'Aigle breccias. Hornfels of the Mont-de-l'Aigle deposit resulted from contact metamorphism by granitic sills at depth, preceded IOCG alteration and mineralization. IOCG mineralization is therefore postdike emplacement, contact metamorphism and epithermal mineralization.

Stevens (1986) proposed that the hydrothermal fluids that formed the epithermal mineralization were likely driven by heat from a deep-seated pluton that also uplifted Dome Lemieux. Fe, Cu, Co enrichment, and sulfur isotope composition at the Mont-de-l'Aigle deposit suggest involvement of a mafic to intermediate magma (Pollard 2002; Thorkelson et al. 2001). Pollard (2002) concluded from several lines of evidence that fluids derived from contemporaneous magmas played a major role in the formation of sodic–calcic alteration and Cu–Au mineralization. The deep-seated pluton might have exsolved magmatic fluids (Sillitoe 2003) that migrated upward, such that intense albitization is limited around mineralization at the Mont-de-l'Aigle deposit.

Preexisting structures are commonly reactivated in IOCG systems and new fracture systems tend to exploit competency contrasts and areas where strain partitioning created zones of brecciation in competent rocks (Pollard 2002). The Mont-de-l'Aigle area contains several faults that are interpreted to have been active during and after the Acadian Orogeny (Pilote and Lachance 2003). The close spatial relationship between IOCG mineralization, brittle faults, and intrusions at the Mont-de-l'Aigle deposit (Figs. 2 and 8) indicates that mineralization and magma emplacement were channeled primarily by these brittle faults. Likewise, the faults could have facilitated inflow of surficial fluids and upflow of hypersaline fluid from depth.

In IOCG deposits, the H_2O–CO_2–salt fluids may unmix due to decreasing pressure and/or temperature, resulting in partitioning of CO_2 to the vapor phase and of salt to the liquid phase to form a hypersaline magmatic fluid (Bowers and Helgeson 1983; Pollard 2002). Oliver et al. (2004) suggested that highly saline fluids may exsolve from crystallization of intermediate to felsic magma and then

evolve along a down-temperature path (Cline and Bodnar 1991), as proposed for the source of metal and brine at La Candelaria (Marschick and Fontboté 2001; Marschick et al. 2003), Andean (Sillitoe 2003), and Cloncurry IOCG deposits (Mark et al. 2002; Pollard 2001). Pollard (2002) proposed that albitization results from unmixing between H_2O–CO_2–salt vapor and liquid phases and will give way at lower temperatures to potassic alteration due to decrease in Na/(Na + K) with decreasing temperature and salinity (Orville 1963; Pollard 2002). If cooling is rapid such as at shallow levels, the high Na/(Na + K) in the original carbonic fluid may yield no sodic alteration because a decrease in temperature promotes potassic alteration (Orville 1963; Pollard 2002). Therefore, early albitization overprinted by potassic alteration at the Mont-de-l'Aigle deposit could be interpreted to reflect evolution of a CO_2-bearing hot magmatic fluid to a cooler fluid, either by convection or as a result of mixing with other cooler fluids.

The alteration and paragenetic sequence of the Mont-de-l'Aigle deposit indicates variation in temperature, pH, and oxygen fugacity that is thought to have played a major role in initiating deposition of metals. Ore deposition at the Mont-de-l'Aigle deposit could have resulted from mixing of a high temperature, CO_2-rich, saline magmatic fluid with a lower temperature, more oxidized, low salinity fluid, perhaps meteoritic water. Fluid reduction by wall-rock reaction with organic matter in carbonate rocks could decrease oxygen fugacity as proposed for the Sullipek deposit (Wares 1986) and induce pseudomorphic replacement of early hematite by magnetite. Mixing can occur repetitively in a high-level setting such as found at Olympic Dam (Haynes et al. 1995; Pollard 2002). The occurrence of late dolomite ± hematite and barite veins at Mont-de-l'Aigle suggests that oxidized fluid became dominant in the waning stages of the system, such as documented for Olympic Dam (Haynes et al. 1995).

Conclusions

The Mont-de-l'Aigle mineralization shares a number of characteristics that are common to oxidized IOCG deposits formed at shallow (≤5 km) depths (Hitzman et al. 1992; Marschick and Fontboté 2001; Pollard 2002; Hitzman 2000; Thorkelson et al. 2001; Sillitoe 2003; Hunt et al. 2005; Williams et al. 2005). These are:

1. Veins, stockworks, and breccias cemented by hematite, quartz, pyrite, chalcopyrite, dolomite, and magnetite (mushketovite).
2. Abundant hematite−quartz cemented breccia.
3. Close spatial relationship between mineralization, intrusions, and faults.
4. Replacement of hematite by magnetite (mushketovite) produced by the reduction of oxidized magmatic fluid via interaction with carbonate host rocks or/and by increased temperature of the hydrothermal system perphaps by successive pulses of ascending magmatic fluid.
5. An intracontinental orogenic collapse tectonic setting accompanied by bimodal transitional magmatism perhaps during subduction-related extension. Felsic intrusions from the Mont-de-l'Aigle deposit are geochemically similar to those associated with porphyry and skarn copper deposits in the Gaspé Peninsula but are older than intrusions at Mines Gaspé and Sullipek deposits;
6. Sulfur isotope composition, Fe, Co, and Cu enrichment and, sodic and potassic alteration suggest the evolvement of magmatic fluids. Oxygen isotope compositions indicate that the $\delta^{18}O$ of the fluid from which quartz precipitated indicating a meteoric or seawater that had equilibrated with the country rocks. The temperature of the hydrothermal system as determined from chlorite geothermometry ranged from 280 to 347°C and has salinity ranging between 0 and 26 wt% NaCl equivalent (Stevens 1986). Chlorite temperatures are comparable to isotope equilibrium temperature from quartz−hematite pairs, 251−328°C. These data support a fluid mixing model, a saline magmatic fluid, and a low salinity surficial fluid.

The Mont-de-l'Aigle deposit is considered to be a rare example of a Paleozoic IOCG deposit formed at shallow levels and hosted by carbonate rocks. Mineralization has a strong spatial relationship with faults and mafic to felsic intrusions (Figs. 2 and 8). Relations with felsic intrusions need to be investigated in more detail because the copper deposits of the Gaspé Peninsula have a strong spatial and genetic relationship with similar, albeit younger, felsic magmatism. The Mont-de-l'Aigle deposit perhaps bears a spatial and temporal relationship with the Cu−Mo porphyry deposits of Mines Gaspé and Sullipek, similar to that of Mesozoic IOCG and Cu−Mo porphyry deposits in the Andes.

Acknowledgements This manuscript constitutes a portion of a M. Sc. memoir completed at Université Laval. This research project has been supported by Ressources Appalaches and the Natural Science and Engineering Council of Canada Discovery Grant to G. Beaudoin. A. Ross, S. Lachance, P. Pilote (MRNFP), and M. Malo (INRS-ETE) are acknowledged for their helpful discussions on the geology and metallogeny of the Gaspé Peninsula. D. Lentz, L. Meinert, J. Walker, and an anonymous reviewer are thanked for their constructive reviews, which significantly improved the manuscript.

Appendix

Table 10 Major and trace element composition of intrusions from the Mont-de-l'Aigle deposit, Gaspé Peninsula, Quebec

Type	1					2				
Sample #	217894	217896	218865	218868	218893	218801	218802	218803	218861	218864
DDH			F02–03	F02–03	F02–04	F02–07	F02–07	F02–07	F03–12	F02–03
SiO_2 (wt%)	50.13	33.96	40.32	44.39	42.01	31.75	38.76	47.29	50.57	33.69
Al_2O_3	7.01	5.71	17.57	14.48	15.63	14.79	13.47	13.63	13.73	17.20
TiO_2	0.71	0.62	1.98	1.75	1.71	1.99	2.24	2.13	2.12	2.53
Fe_2O_3[a]	31.85	49.45	17.62	16.65	17.89	25.78	23.17	16.08	15.00	21.79
MnO	0.20	0.16	0.27	0.29	0.20	0.48	0.41	0.23	0.23	0.34
MgO	3.33	2.53	8.95	9.41	9.93	14.27	11.67	8.94	5.64	12.13
CaO	0.23	0.16	0.46	2.05	0.66	0.83	0.83	1.55	1.20	0.63
Na_2O	0.06	0.08	0.41	2.85	0.54	0.03	0.07	0.22	0.16	0.26
K_2O	0.08	0.08	5.14	0.13	3.62	0.02	0.47	2.82	4.71	2.28
P_2O_5	0.17	0.13	0.29	0.22	0.22	0.43	0.48	0.46	0.86	0.42
LOI	5.17	6.35	5.70	6.79	5.98	8.61	7.21	5.86	4.43	7.46
Total	98.95	99.22	98.71	99.02	98.37	98.98	98.79	99.23	98.63	98.73
Ba (ppm)	8	8	2060	35	1380	5	116	759	1780	1180
Co	143	220	25	57	53	56	51	67	ND	33
Cu	3	4	ND	ND	ND	ND	ND	ND	21	ND
Nb	13	10	9	7	8	18	21	19	6	12
Ni	25	20	51	88	165	56	48	53	87	51
Rb	4	3	97	3	83	ND	13	68	87	38
Sr	6	6	133	56	76	17	24	158	76	72
Th	1	1	2	1	1	4	5	4	6	2
V	82	92	247	225	209	228	222	238	148	307
Y	11	13	30	22	24	26	24	31	40	42
Zr	85	72	150	125	134	189	218	200	232	205
La	9.3	8.4	16.0	11.3	13.5	43.0	39.7	36.1	30.5	30.5
Ce	20.4	18.5	37.3	25.4	30.1	79.0	75.3	68.4	66.1	62.8
Pr	2.3	2.0	4.8	3.4	3.9	9.0	8.6	7.7	8.2	7.9
Nd	9.5	8.3	21.1	15.4	16.3	36.3	35.7	32.3	34.6	34.4
Sm	2.2	2.1	5.1	4.0	3.9	7.3	7.5	7.0	7.5	7.9
Eu	0.5	0.6	1.9	1.6	1.4	2.8	2.8	2.4	1.8	3.5
Gd	2.1	2.2	5.2	4.2	4.1	6.8	6.9	6.8	7.7	8.1
Tb	0.4	0.4	0.9	0.8	0.8	1.0	1.1	1.2	1.4	1.4
Dy	2.1	2.5	5.5	4.7	4.6	5.3	5.7	6.3	8.5	8.1
Ho	0.4	0.5	1.1	0.9	0.9	1.0	1.0	1.2	1.8	1.6
Er	1.2	1.5	3.5	2.9	2.8	3.0	3.1	3.5	5.4	4.8
Tm	0.2	0.2	0.5	0.4	0.4	0.5	0.5	0.5	0.8	0.7
Yb	1.2	1.3	3.1	2.7	2.7	2.9	3.1	3.3	4.7	4.1
Lu	0.2	0.2	0.5	0.4	0.4	0.4	0.5	0.5	0.7	0.6

ND Not detected
[a]Total Fe as Fe2O3

					3					
218866 F02–03	218874 F02–10	218876 F02–11	218877 F02–11	218878 F02–12	218830 F02–07	218831 F02–07	218833 F02–07	218834 F02–07	218835 F02–07	218836 F02–07
26.98	39.38	43.13	47.11	35.34	55.99	48.27	51.76	51.38	37.45	48.79
16.42	13.97	12.94	13.40	15.70	15.50	15.63	15.04	15.10	15.76	15.70
2.45	3.21	2.68	2.78	2.05	1.40	1.98	2.06	2.12	2.23	2.16
28.50	21.54	18.12	14.47	27.88	10.93	14.05	12.14	15.34	24.77	15.15
0.32	0.26	0.15	0.23	0.31	0.14	0.24	0.17	0.18	0.34	0.19
14.59	9.83	4.90	6.34	7.78	3.76	5.06	5.46	4.98	7.27	4.85
0.74	1.55	7.09	6.39	0.95	1.17	2.07	1.69	1.10	1.02	0.93
0.05	1.85	3.84	4.62	0.15	4.97	5.61	3.29	4.43	0.85	0.44
ND	0.07	0.10	0.05	1.88	1.52	0.05	2.64	0.40	2.38	6.42
0.51	0.61	0.43	0.42	0.36	0.66	0.63	0.63	0.61	0.69	0.65
8.37	6.63	5.74	3.50	6.86	3.26	5.29	4.50	4.23	6.21	3.80
98.93	98.88	99.10	99.30	99.25	99.29	98.89	99.38	99.87	98.97	99.09
14	11	11	10	656	576	15	956	112	358	1950
36	29	24	39	ND	22	33	21	31	54	20
ND	ND	ND	ND	97	ND	ND	26	18	ND	ND
21	23	18	18	7	24	22	21	19	21	20
62	52	56	64	99	ND	ND	ND	25	27	33
3	ND	9	3	38	29	ND	53	7	33	119
36	39	270	274	28	139	64	172	100	35	107
5	3	2	2	4	5	5	4	5	5	5
268	286	331	338	229	75	167	185	179	183	198
17	26	ND	ND	9	ND	1	ND	3	5	4
38	52	38	34	31	52	48	48	42	42	50
84	133	53	45	59	56	76	70	37	84	58
229	264	218	215	222	365	338	310	306	346	327
34.8	70.3	25.6	23.7	32.5	46.3	45.8	39.4	32.5	37.4	38.0
70.9	137.6	56.7	53.7	70.1	100.3	96.7	86.7	72.9	82.8	83.0
8.3	15.9	7.4	7.0	8.5	12.3	11.9	10.7	9.1	10.3	10.3
33.5	62.3	31.5	30.0	33.0	50.4	49.3	44.8	37.7	42.7	42.8
7.0	12.8	7.4	7.3	6.9	11.1	10.9	10.2	8.4	9.2	9.3
2.5	3.3	2.7	2.4	1.6	2.3	2.8	2.6	1.4	1.6	1.8
6.7	11.3	7.6	7.2	6.2	10.5	10.6	10.0	8.1	8.5	9.1
1.1	1.8	1.3	1.3	1.1	1.9	1.8	1.8	1.4	1.4	1.7
6.9	9.5	7.4	7.1	6.1	10.6	9.9	9.8	7.6	7.9	9.5
1.4	1.9	1.4	1.3	1.2	2.1	1.9	2.0	1.5	1.6	2.0
4.4	5.8	4.0	3.9	3.7	6.5	5.9	6.0	4.8	5.2	6.0
0.7	0.8	0.6	0.6	0.6	1.0	0.9	0.9	0.7	0.8	0.9
4.0	5.0	3.7	3.6	3.8	6.0	5.6	5.3	4.4	5.1	5.4
0.6	0.7	0.5	0.5	0.5	0.9	0.8	0.8	0.7	0.8	0.8

				4						
218858 F03–09	218859 F03–11	218860 F03–19	218871 F02–08	217898	218837 F02–07	218838 F02–07	218839 F02–07	218840 F02–07	218841 F02–07	218851 F03–17
52.56	53.65	50.07	50.45	77.24	73.21	73.23	82.22	58.83	73.45	78.03
15.45	11.68	15.22	15.49	10.36	10.71	11.64	10.56	9.66	11.63	11.80
	2.13	2.27	2.12	0.11	0.14	0.15	0.13	0.12	0.15	0.15
11.37	14.11	14.44	11.57	2.91	6.78	4.42	0.81	17.31	3.49	1.81
	0.25	0.20	0.20	0.04	0.09	0.08	0.01	0.26	0.04	0.03
4.98	8.26	4.85	5.36	0.81	2.48	2.43	0.40	5.65	1.42	1.24
0.93	1.00	0.92	2.35	0.04	0.14	0.11	0.13	0.53	0.09	0.12
0.92	0.66	0.38	3.50	0.79	0.13	0.43	0.14	0.10	1.18	0.15
6.10	1.32	5.97	2.89	6.88	3.46	3.79	3.45	1.50	6.32	4.20
0.65	0.69	0.63	0.63	0.02	0.02	0.02	0.04	0.03	0.03	0.03
3.61	5.32	4.13	4.80	0.69	2.81	2.93	2.08	5.00	1.30	2.55
98.88	99.05	99.07	99.35	99.88	99.96	99.24	99.96	98.98	99.11	100.09
2360	560	2680	959	8	979	1520	708	836	3000	1150
15	16	18	ND	3000	13	6	2	36	6	1
ND	ND	ND	13	5	ND	ND	56	12	ND	ND
20	22	20	6	26	16	16	17	15	19	18
ND	ND	ND	46	2	ND	ND	ND	ND	ND	ND
115	23	124	46	115	93	93	98	33	136	107
109	33	169	106	39	67	77	45	52	143	59
5	5	5	5	18	15	16	15	14	18	18
190	179	216	188	ND	16	14	9	8	9	11
7	5	1	2	2	2	ND	1	1	ND	ND
41	46	48	50	15	13	17	18	12	25	26
75	92	51	ND	ND	59	ND	ND	135	ND	ND
321	365	311	298	103	100	101	99	86	110	118
29.4	32.4	32.6	35.0	15.3	15.7	29.0	29.4	11.0	32.8	30.4
66.0	74.3	73.7	77.2	36.4	30.6	56.4	56.6	21.5	60.0	58.2
8.2	9.5	9.3	9.7	3.4	3.3	5.9	5.8	2.3	6.1	5.9
34.2	39.7	39.6	41.1	11.4	11.3	20.0	19.2	8.1	20.8	20.0
7.5	8.8	9.3	9.7	2.3	2.2	3.6	3.6	1.7	3.8	3.9
1.0	1.7	2.0	2.8	0.3	0.3	0.5	0.3	0.3	0.4	0.4
7.4	8.3	9.3	10.1	1.7	1.8	2.7	2.8	1.7	3.6	3.5
1.3	1.4	1.6	1.7	0.3	0.3	0.5	0.5	0.4	0.7	0.7
7.6	8.5	9.2	9.9	2.1	2.1	2.9	3.2	2.1	4.2	4.2
1.6	1.8	1.9	2.0	0.5	0.5	0.6	0.7	0.5	0.9	0.9
5.2	6.0	5.7	6.0	2.2	1.7	2.2	2.3	1.6	3.0	3.0
0.8	0.9	0.8	0.9	0.4	0.3	0.4	0.4	0.3	0.5	0.5
4.7	5.7	5.1	5.4	3.0	2.3	2.7	2.8	2.1	3.6	3.3
0.7	0.8	0.8	0.80	0.4	0.4	0.4	0.4	0.3	0.5	0.5

4									
218852 F03–14	218863 F03–12	218870 F02–08	218872 F02–09	218875 F02–10	218879 F02–12	218886 F03–13	218887 F03–13	218890 F03–13	220574
76.43	74.57	74.32	75.17	75.44	73.72	75.75	75.83	76.45	80.54
10.38	10.13	11.01	11.30	10.71	10.76	10.94	10.89	10.32	8.28
0.13	0.14	0.17	0.16	0.16	0.16	0.14	0.13	0.13	0.12
3.40	6.60	5.91	4.72	2.51	5.10	2.86	3.14	2.73	3.19
0.06	0.10	0.09	0.05	0.03	0.07	0.04	0.05	0.04	0.02
0.79	2.10	2.28	1.70	0.68	1.80	0.72	0.96	0.92	0.45
0.10	0.09	0.20	0.13	0.43	0.40	0.07	0.08	0.17	0.12
0.27	0.55	0.09	0.14	0.68	0.20	0.48	0.43	0.20	1.36
7.22	3.58	3.28	4.28	7.40	5.57	7.67	7.55	7.44	3.43
0.03	0.04	0.04	0.04	0.04	0.03	0.03	0.03	0.03	0.03
0.95	2.07	2.82	2.26	1.71	2.04	0.78	0.91	1.47	1.69
99.76	99.98	100.22	99.95	99.78	99.85	99.47	100.00	99.91	99.21
2070	1370	1010	1880	3270	2490	2140	2280	2880	844
8	12	3	6	2	9	15	12	7	20
ND	28	ND	ND	ND	34	11	37	19	51
16	15	16	17	26	17	16	16	15	13
ND	ND	ND	ND	ND	ND	ND	ND	ND	5
140	78	74	97	105	119	151	142	136	84
53	63	91	93	60	126	74	92	125	171
17	15	17	18	24	16	17	17	16	12
8	11	10	11	8	10	8	7	7	12
ND	ND	ND	ND	ND	ND	ND	ND	ND	2.7
23	17	14	27	20	20	14	16	14	11
ND	ND	ND	ND	ND	ND	ND	ND	ND	17
97	97	101	106	99	100	99	97	92	81
29.7	30.4	22.4	31.7	29.3	32.8	11.2	19.4	12.3	9.7
56.8	57.3	44.7	59.8	56.4	60.7	22.6	38.8	24.6	17.3
5.8	5.9	4.6	6.2	5.7	6.3	2.4	4.1	2.6	2.2
19.9	19.9	15.6	20.9	18.8	21.1	8.6	14.1	9.2	7.3
3.9	3.7	2.9	4.2	3.5	3.7	1.7	2.6	1.9	1.5
0.5	0.4	0.4	0.5	0.5	0.4	0.2	0.3	0.3	0.2
3.4	3.0	2.3	3.8	3.0	3.2	1.6	2.1	1.6	1.6
0.6	0.5	0.4	0.7	0.6	0.6	0.3	0.4	0.3	0.3
3.9	3.2	2.5	4.6	3.7	3.8	2.2	2.6	2.2	1.9
0.8	0.7	0.6	1.0	0.8	0.8	0.5	0.6	0.5	0.4
2.7	2.2	1.9	3.2	3.0	2.5	1.9	2.1	1.8	1.4
0.4	0.4	0.3	0.5	0.5	0.4	0.4	0.4	0.3	0.3
2.9	2.5	2.3	3.4	3.7	2.9	2.6	2.7	2.3	1.9
0.5	0.4	0.4	0.5	0.6	0.4	0.4	0.4	0.4	0.3

References

Allcock JB (1982) Skarn and porphyry copper mineralization at Mines Gaspé, Murdochville, Quebec. Econ Geol 77: 971–999

Barrett TJ, MacLean WH (1994) Chemostratigraphy and hydrothermal alteration in exploration for VHMS deposits in greenstones and younger volcanic rocks. In: Lentz DR (ed) Alteration and alteration process associated with ore-forming systems. Geological Association of Canada (Short Course Notes 11), pp 433–467

Barton MD, Johnson DA (1996) Evaporitic source model for igneous-related Fe oxide–(REE–Cu–Au–U) mineralization. Geology 24:259–262

Bédard JH (1986) Pre-Acadian magmatic suites of the southeastern Gaspé Peninsula. Geol Soc Amer Bull 97:1177–1191

Bellehumeur C, Valiquette G (1993) Synthèse métallogénique du centre nord de la Gaspésie. Ministère de l'Énergie et des Ressources du Québec, ET 92-03, p 63

Bernard J, Beaudoin G, Ross A, Hupé A, Simard M, Malo M (2005) Origine des brèches à hématite de la propriété du Mont-de-l'Aigle en Gaspésie. GAC–MAC annual meeting, Abstracts with Program, p 16

Bourque PA, Brisebois D, Malo M (1995) Middle Paleozoic rocks of Québec and adjacent New Brunswick. In: Williams H (ed.) Geology of Appalachian–Caledonian Orogen in Canada and Greenland, Geological Society of America, Decade of North American Geology, p F-1

Bowers TS, Helgeson HC (1983) Calculation of the thermodynamic and geochemical consequences of non-ideal mixing in the system H_2O–CO_2–NaCl on phase relations in geologic systems: equation of state for H_2O–CO_2–NaCl fluids at high pressures and temperatures. Geochim Cosmochim Acta 47:1247–1275

Cathelineau M (1988) Cation site occupancy in chlorites and illites as a function of temperature. Clay Miner 23:471–485

Cathelineau M, Nieva D (1985) A chlorite solid solution geothermometer: the Los Azufres (Mexico) geothermal system. Contrib Mineral Petrol 91:235–244

Clayton RN, Mayeda TK (1963) The use of bromide pentafluoride in the extraction of oxygen from oxides and silicates for isotopic analysis. Geochim Cosmochim Acta 27:43–52

Clayton RN, O'Neil JR, Mayeda TK (1972) Oxygen isotope exchange between quartz and water. J Geophys Res 77:3057–3067

Cline JS, Bodnar RJ (1991) Can economic porphyry copper mineralization be generated by a typical calc–alkaline melt? J Geophys Res 96:8113–8126

Corbett GJ, Leach TM (1998) Controls on hydrothermal alteration and mineralization. In: Corbett GJ, Leach TM (eds) Southwest Pacific rim gold–copper systems: structure, alteration and mineralization. Soc Econ Geol Spec Publ 6, pp 69–82

Creaser RA (1996) Petrogenesis of a Mesoproterozoic quartz latite–granitoid suite from the Roxby Downs area, South Australia. Precambrian Res 79:371–394

De Caritat P, Hutchson I, Walshe JL (1993) Chlorite geothermometry: a review. Clays Clay Miner 41(2):219–239

de Haller A (2000) The Raúl-Condestable iron oxides–Cu–Au deposit, Lima department, Perú: preliminary results. Annual GEODE–Fennoscandian shield field workshop on Paleoproterozoic and Archean greenstone belts and VMS districts in the Fennoscandian shield, 2nd, Gällivare-Kiruna, Sweden, August 28–September 1 2000, Research report, pp 8–11

de Römer HS (1974) Geology and age of some plutons in north-central Gaspé, Canada. Can J Earth Sci 11:570–582

Dilles JH, Einaudi MT (1992) Wall-rock alteration and hydrothermal flow paths about the Ann-Mason porphyry copper deposit—Nevada: a 6 km vertical reconstruction. Econ Geol 87:1963–2001

Doyon M (1988) Synthèse géologique des roches volcaniques du Centre Nord de la Gaspésie. Master thesis. École Polytechnique, Montréal, p 244

Doyon M (1992) Géochimie et environnement tectono-stratigraphique des roches volcaniques du centre-nord de la Gaspésie, Québec. Ph.D. thesis. École Polytechnique de Montréal, p 254

Doyon M, Berger J (1997) Distribution et contrôles structuraux des roches magmatiques Siluro–Dévoniennes de la Gaspésie. Ministère des Ressources Naturelles du Québec, ET 97-01, p 31

Doyon M, Dalpé C (1993) Roches magmatiques Siluro–Dévoniennes de la Gaspésie, MB 93-16. Ministère des Ressources naturelles, Québec, p 137

Doyon M, Valiquette G (1991) Roches magmatiques du centre nord de la Gaspésie, ET 90-03. Ministère de l'Énergie et des Ressources, Québec, p 67

Förster H (1990) Scapolite-analcite-bearing magnetite ore from Seh Chahoon, central Iran. 8th IAGOD Symposium, Program with Abstracts, Ottawa, Canada, August, p A196

Förster H, Knittel U (1979) Petrographic observation on a magnetite deposit at Mishdovan, central Iran. Econ Geol 74:1485–1510

Gentile F (1969) Étude stratigraphique et structurale du dôme de Lemieux, comté de Gaspé-Nord, Québec. Mémoire de maîtrise, département de géologie, Université de Montréal, p 86

Gosselin P (2000) Analyse structurale et métallogénique des minéralisations nickélifères le long de la faille Shickshock-Sud, Gaspésie. Mémoire de maîtrise, INRS-Géoressources (Université du Québec), p 147

Grant JA (1986) The isocon diagram—a simple solution to Gresens' equation for metasomatic alteration. Econ Geol 81:1976–1982

Guilbert JM, Park CF (1986) The Geology of ore deposits. WH Freeman and Company, New York, p 985

Haynes DW, Cross KC, Bills RT, Reed MH (1995) Olympic Dam ore genesis: a fluid-mixing model. Econ Geol 90:281–307

Hey MH (1954) A new review of chlorites. Mineral Mag 30:277–292

Helvaci C (1984) Apatite-rich iron deposits of the Avnik (Bignol) region, southeasthern Turkey. Econ Geol 79:354–371

Hitzman MW (2000) Iron oxide–Cu–Au deposits: what, where, when, and why. In: Porter TM (ed) Hydrothermal iron oxide copper–gold and related deposits: a global perspective. Australian Mineral Foundation, Adelaide, pp 9–25

Hitzman MW, Oreskes N, Einaudi MT (1992) Geological characteristics and tectonic setting of Proterozoic iron oxide (Cu–U–Au–REE) deposits. Precambrian Res 58:241–287

Hopper D, Correa A (2000) The Panulcillo and Teresa de Colmo copper deposits: two contrasting examples of Fe–Ox Cu–Au mineralization from the Coastal Cordillera of Chile. In: Porter TM (ed) Hydrothermal iron oxide copper–gold and related deposits: a global perspective, vol 1. PGC Publishing, Adelaide, pp 177–189

Hunt J, Baker T, Thorkelson D (2005) Regional-scale Proterozoic IOCG-mineralized breccia systems: examples from the Wernecke Mountains, Yukon, Canada. Miner Depos 40:492–514

Irvine TN, Baragar WRA (1971) A guide to the classification of the common volcanic rocks. Can J Earth Sci 8:523–548

Kajiwara Y, Krouse HR (1971) Sulfur isotope partitioning in metallic sulfide systems. Can J Earth Sci 8:1397–1408

Lane RA (1990) Geologic setting and petrology of the Proterozoic Ogilvie Moutain breccias of the Coal Creek Inlier, southern Ogilvie Mountains, Yukon Territory. Ph.D. dissertation. University of British Columbia, Vancouver, B.C., p 223

Laurent R, Dostal J (1990) The Siluro–Devonian basalt–tholeiitic andesite association from the Gaspé Peninsula. In: Malo M, Lavoie D, Kirkwood D (eds) Programmes et résumés du séminaire sur les Appalaches du segment Québec–Maine–Nouveau–Brunswick. Commission géologique du Canada document public 2235, pp 67–71

Laznicka P, Edwards RJ (1979) Dolores Creek, Yukon—a disseminated copper mineralization in sodic metasomatites. Econ Geol 74:1352–1370

Malo M (2001) Late Silurian–Early Devonian tectono-sedimentary history of the Gaspe Belt in the Gaspe Peninsula: from a transtensional Salinic basin to an Acadian foreland basin. In: Lavoie D, Bourque PA (eds) Hydrocarbon plays in the Silurian–Devonian Gaspe Belt, Quebec, Appalachians. Bull Can Pet Geol 49 (2), pp 202–216

Malo M, Bourque PA (1993) Timing of deformation events from Late Ordovician to Mid-Devonian in the Gaspé Peninsula. In: Roy DC, Skehan JW (eds) The Acadian orogeny: recent studies in New England, Maritime Canada, and the autochthonous foreland. Geol Soc Am Spec Pap 275, pp 101–122

Mark G, Oliver NHS, Williams PJ, Valenta RK, Crookes RA (2002) The evolution of the Ernest Henry hydrothermal system. In: Porter TM (ed) Hydrothermal iron oxide copper–gold and related deposits: a global perspective, vol 2. PGC Publishing, Adelaide, pp 132–136

Mark G, Williams PJ, Boyce AJ (2004) Low-latitude meteoric fluid flow along the Cloncurry Fault, Cloncurry district, NW Queensland, Australia: geodynamic and metallogenic implications. Chem Geol 207:117–132

Marschick R, Fontboté L (1996) Copper (–Iron) mineralization and superposition of alteration events in the Punta del Cobre belt, Northern Chile. In: Camus F, Sillitoe RH, Peterson R (eds) Andean copper deposits: new discoveries, mineralization, styles and metallogeny. Soc Econ Geol Spec Publ 5, pp 171–190

Marschick R, Fontboté L (2001) The Candelaria–Punta del Cobre iron oxide Cu–Au(–Zn–Ag) deposits, Chile. Econ Geol 96:1799–1826

Marschick R, Fontignie D, Chiaradia M, Voldet P (2003) Geochemical and Sr–Nd–Pb–O isotope composition of granitoids of the Early Cretaceous Copiacó plutonic complex (27° 30′S), Chile. JS Am Earth Sci 16:381–398

McDonough WF, Sun SS (1995) The composition of the Earth. Chemical evolution of the mantle. Chem Geol 120:223–253

Meinert LD (1993) Igneous petrogenesis and skarn deposits. In: Kirham RV, Sinclair WD, Thorpe RI, Duke JM (eds) Mineral deposit modelling. Geological Association of Canada, Special Paper 40:569–583

Oliver NHS, Cleverley JS, Mark G, Pollard PJ, Fu B, Marshall LJ, Rubenach MJ, Williams PJ, Baker T (2004) Modeling the role of sodic alteration in the genesis of iron–oxide–copper–gold deposits, eastern Mount Isa block, Australia. Econ Geol 99:1145–1176

Orville PM (1963) Alkali ion exchange between vapour and feldspar phases. Am J Sci 261:201–237

Pearce JA, Harris NBW, Tindle AG (1984) Trace element discrimination diagrams for the tectonic interpretation of granitic rocks. J Petrol 25:956–983

Pilote P (2005) Métallogénie de la région du Dôme de Lemieux–partie centre–nord de la Gaspésie. Ministère des Ressources naturelles et Parcs du Québec, ET 2004-05, p 53

Pilote P, Lachance S (2003) Géologie et potentiel minéral de la région du lac Sainte-Anne (22B/16-200-0102). Ministère des Ressources naturelles et parcs du Québec, DV 2003-09, 36

Pollard PJ (2001) Sodic (-calcic) alteration in Fe–oxide–Cu–Au districts: an origin via unmixing of magmatic H_2O–CO_2–NaCl ± $CaCl_2$–KCl fluids. Miner Depos 36:93–100

Pollard PJ (2002) Evidence of a magmatic fluid and metal source for Fe-oxide Cu–Au mineralization. In: Porter TM (ed) Hydrothermal iron oxide copper–gold and related deposits: a global perspective, vol 1. PGC Publishing, Adelaide, pp 27–41

Pollard PJ, Mark G, Mitchell LC (1998) Geochemistry of post-1540 Ma granites in the Cloncurry district, northwest Queensland. Econ Geol 93:1330–1344

Ray GE, Webster ICL (2000) Characteristics of the Fe oxide–Cu–Au family and the potential for these deposits in British Columbia. In: Iron oxide copper–gold deposits: separating fact from fantasy. Short course notes. Vancouver Mining Association, BC Yukon Chamber Mines, Vancouver, pp F1–F47

Requia K, Stein H, Fontboté L, Chiaradia M (2003) Re–Os and Pb–Pb geochronology of the Archean Salobo iron oxide copper–gold deposit, Carajás mineral province, northern Brazil. Miner Depos 38:727–738

Rotherham JF (1997a) Origin and fluid chemistry of the Starra ironstones and high-grade Au–Cu mineralization, Cloncurry district, Mount Isa inlier, Australia. Ph.D. thesis, Townsville, James Cook University, p 251

Rotherham JF (1997b) A metasomatic origin for the iron–oxide Au–Cu Starra orebodies, Eastern Fold Belt, Mount Isa Inlier. Miner Depos 32:205–218

Schmidt Mumm A, Wolfgramm M (2004) Fluid systems and mineralization in the north German and Polish basin. Geofluids 4:315–328

Shelton KL (1983) Composition and origin of ore-forming fluids in a carbonate-hosted porphyry copper and skarn deposit: a fluid inclusion and stable isotope study of the Mines Gaspé, Quebec. Econ Geol 78:387–421

Shelton KL, Rye DM (1982) Sulfur isotopic compositions of ores from Mines Gaspé, Quebec: an example of sulfate–sulfide isotopic disequilibrium with applications to other porphyry-type deposits. Econ Geol 77:1688–1709

Sillitoe RH (2003) Iron oxide–copper–gold deposits: an Andean view. Miner Depos 38:787–812

Stephenson EM, Meinert LD, Mortensen JK, Hussey J (1998) Age and skarn alteration of the Porphyry Mountain Cu–Mo deposit, Mines Gaspe, Quebec. Geol Am, 1998 annual meeting, Abstracts with Programs—Geological Society of America 30, p 372

Stevens K (1986) Fluid inclusion and geological studies on the Zn–Pb–Cu vein system at Lemieux Dome, Gaspé, Québec. M.Sc. thesis, McGill University, Montréal, Québec, p 150

Swinden HS, Dunsworth SM (1995) Chapter 9—Metallogeny. In: Williams H (ed) Geology of the Appalachian–Caledonian orogen in Canada and Greenland, Geological Survey of Canada, Geology of Canada 6, pp 681–814

Taghizadeh N (1977) The iron deposits of Iran. In: Walther HW, Zitzmann A (eds) The iron ore deposits of Europe and adjacent areas. International Geology Congress, Hannover, pp 199–202

Tallarico FHB, Figueiredo BR, Groves DI, Kositcin N, McNaughton IRF, Rego JL (2005) Geology and SHRIMP U–Pb geochronology of the Igarapé Bahia deposit, Carajás copper–gold belt, Brazil: an Archean (2.57 Ga) example of iron-oxide Cu–Au (U–REE) mineralization. Econ Geol 100(1):7–29

Thorkelson DJ, Mortensen JK, Davidson GJ, Creaser GA, Perez WA, Abbott JG (2001) Early Mesoproterozoic intrusive breccias in Yukon, Canada: the role of hydrothermal systems in reconstructions of North America and Australia. Precambrian Res 111:31–55

Treuil M, Varet F (1973) Critères volcanologiques, pétrologiques et géochimiques de la genèse et de la différenciation des magmas basaltiques: exemple de l'Afar. Bull Soc Geol Fr 7:506–540

Vila T, Lindsay N, Zamora R (1996) Geology of the Manto Verde copper deposit, northern Chile: a specularite-rich hydrothermal-tectonic breccia related to the Atacama fault zone. In: Camus F, Sillitoe RH, Petersen R (eds) Andean copper deposits: new discoveries, mineralization, styles and metallogeny, Soc Econ Geol Spec Publ 5, pp 157–170

Wares R (1983) Synthèse métallogénique du gîte Sullipek et de ses environs. Ministère de l'Énergie et des Ressources du Québec, DP-83-02, p 1

Wares R (1986) Géologie et métallogénie de la région du gîte de Sullipek, Gaspésie. Ministère de l'Énergie et des Ressources du Québec, ET 86-08, p 92

Whalen JB, Mortensen JK, Roddick C (1991) Implications of U–Pb and K–Ar geochronology for petrogenesis and cooling history of the McGerrigle Mountains plutonic complex, Gaspé, Québec. Can J Earth Sci 28:754–761

Whalen JB, Jenner GA, Gariépy C, Longstaffe FJ (1994) Geochemical and isotopic (Nd, O, and Pb) constraints on granite source in the Humber and Dunnage zones, Gaspésie, Quebec, and New Brunswick: implications for tectonics and crustal structure. Can J Earth Sci 31:323–340

Williams H, Hatcher RD (1983) Appalachian suspect terranes. In: Hatcher RD et al (eds) Contributions to the tectonics and geophysics of mountain chains. Geol Soc Am Memoir 158, pp 33–53

Williams PJ, Pollard PJ (2001) Australian proterozoic iron oxide-Cu-Au deposits: An overview with new metallogenic and exploration data from the Cloncurry district, Northwest Queensland. Explor Min Geol 10:191–213

Williams PJ, Barton MD, Johnson DA, Fontboté L, de Haller A, Mark G, Oliver NHS, Marschik R (2005) Iron oxide copper–gold deposits: geology, space–time distribution, and possibles mode of origin. Econ Geol (100th Anniversary Volume): 371–405

Winchester JA, Floyd PA (1977) Geochemical discrimination of different magma series and their differentiation products using immobile elements. Chem Geol 20:325–343

Winter JD (2001) An introduction to igneous and metamorphic petrology. Prentice Hall, New Jersey, p 697

Zheng Y-F (1991) Calculation of oxygen isotope fractionation in metal oxides. Geochim Cosmochim Acta 55:2299–2300